

Review

# Aerodynamic Characteristics of Wind Turbines Operating under Hazard Environmental Conditions: A Review

Eleni Douvi  and Dimitra Douvi \* 

Department of Mechanical Engineering & Aeronautics, University of Patras, 26504 Rio Achaia, Greece;  
douvi@upatras.gr

\* Correspondence: ddouvi@upatras.gr

**Abstract:** This paper provides a review of the aerodynamic behavior of horizontal axis wind turbines operating in hazardous environmental conditions. Over the past decade, renewable energy use has accelerated due to global warming, depleting fossil fuel reserves, and stricter environmental regulations. Among renewable options, solar and wind energy have shown economic viability and global growth. Horizontal axis wind turbines offer promising solutions for sustainable energy demand. Since wind turbines operate in an open environment, their efficiency depends on environmental conditions. Hazard environmental conditions, such as icing, rainfall, hailstorms, dust or sand, insects' collisions, increased humidity, and sea spray, result in degraded aerodynamic characteristics. The outcome of most studies has been that the airfoils' lift is degraded, and at the same time, drag is increased when wind turbines operate under these conditions. The objective of this review is to improve our comprehension of these crucial aspects so they are taken into account when designing wind turbine blades, and it offers suggestions for future research paths. It serves as a valuable resource that can inspire researchers who are dedicated to enhancing the aerodynamic characteristics of horizontal axis wind turbines.

**Keywords:** aerodynamic characteristics; wind turbine; icing; rainfall; hailstorm; dust; sand; insects; humidity; sea spray



**Citation:** Douvi, E.; Douvi, D. Aerodynamic Characteristics of Wind Turbines Operating under Hazard Environmental Conditions: A Review. *Energies* **2023**, *16*, 7681. <https://doi.org/10.3390/en16227681>

Academic Editors: Shine Win Naung, Mohammad Rahmati and Mahdi Erfanian Nakhchi

Received: 27 September 2023  
Revised: 11 November 2023  
Accepted: 15 November 2023  
Published: 20 November 2023



**Copyright:** © 2023 by the authors. Licensee MDPI, Basel, Switzerland. This article is an open access article distributed under the terms and conditions of the Creative Commons Attribution (CC BY) license (<https://creativecommons.org/licenses/by/4.0/>).

## 1. Introduction

Over the past decade, the utilization of renewable energy sources (RES) has witnessed a significant acceleration in response to the escalating threats posed by global warming, the reduction in fossil fuel reservoirs, and the implementation of stricter environmental regulations in the global energy market and society [1]. Among all the available renewable energy options, solar energy and wind energy have emerged as the most economically viable sources, experiencing rapid growth on a global scale [2]. Figure 1 illustrates the global distribution of operational and under construction wind farms with capacities of 10 MW or more.

After experiencing a consecutive decline over the past two years, the capacity additions for onshore wind energy are projected to witness a remarkable recovery in 2023, with an anticipated increase of 70% to reach a historic milestone of 107 GW [3]. This resurgence can primarily be attributed to the successful completion of delayed projects in China that were affected by the COVID-19 restrictions imposed last year. Furthermore, accelerated expansion is expected across Europe and the USA, as the challenges faced in the supply chain have caused project commissioning to be postponed from 2022 to 2023. Conversely, the development of offshore wind energy is not projected to match the unprecedented expansion achieved two years ago, largely due to the limited number of projects currently under construction outside of China.

Two main types of wind turbines exist, categorized based on their rotor structure and position in airflow: horizontal axis wind turbines (HAWTs) and vertical axis wind

turbines (VAWTs). HAWTs have gained significant popularity in the commercial electricity generation sector, owing to a considerable amount of time and effort having been invested in their research and development, due to their higher efficiency. The present review paper primarily examines HAWTs, which enjoy a broader adoption and are commonly employed in wind farms.



**Figure 1.** Worldwide map showing the operating (green) and under construction (yellow) wind farms with capacities equal to or exceeding 10 MW [4].

The efficiency of a HAWT is influenced by numerous variables, including the wind speed during operation, the length of the blades, the height of the tower, the design of the casing, and the environmental conditions in the vicinity, including weather conditions, as well as collisions with birds and insects [5].

The aerodynamics of the blade significantly impacts the performance of a HAWT. Additionally, collisions with birds and insects can disrupt the blade's aerodynamic profile, resulting in increased aerodynamic drag and a subsequent decrease in power generation of up to 50% [6–8]. Moreover, the accumulation of ice on the surface further impacts the HAWT's performance, leading to a potential decrease in power generation ranging from 20% to 50% [6]. Under normal circumstances, the performance of a HAWT is closely linked to the wind speed profile at a specific site. Any variations in wind speed profiles have a substantial impact on turbine performance.

Achieving accurate calculations of HAWT power curves is crucial for power performance testing and annual energy production (AEP) assessments. The presence of icing causes a decrease in the AEP by up to 17% and leads to a reduction in the power coefficient within the range of 20–50% [9]. Rainfall has the potential to induce erosion on the surfaces of HAWT blades, leading to an increase in surface roughness, which eventually increases the aerodynamic drag of the blades [10–15]. Consequently, this leads to a decline in performance and a subsequent loss of energy [10,16]. It is worth noting that erosion on HAWT blades can result in AEP losses of up to 25% [17–20]. Moreover, the accumulation of dirt and insects on the blade surface can result in roughness, leading to a potential decrease of up to 50% in power output [6,21,22]. The effects of increased surface roughness, resulting from factors such as sand or insect impacts, as well as erosion caused by rain, on the power output of HAWTs were examined in [23].

Hence, it is imperative to comprehensively examine all the variables influencing HAWT aerodynamic characteristics and discuss potential solutions. HAWTs offer a promising solution to address the growing demand for sustainable energy in the future, presenting an appealing technology for harnessing wind energy and converting it into electricity or other useful forms. This review aims to enhance our understanding of the key parameters that must be considered during HAWT blade design and provides recommendations for future research areas.

## 2. Aerodynamic Performance of Wind Turbines

The blades of the wind turbine harness the kinetic energy of the incoming wind and convert it into mechanical energy stored in the shaft. The shaft is then linked to an electrical generator, which produces electricity. The power output of a wind turbine is determined by the speed of the incoming wind, the size of the turbine, and the area it sweeps. The maximum amount of kinetic energy extractable from the wind is approximately 59.3% of the total available wind power, according to the Betz limit [24]. The power generated by a wind turbine ( $P$ ) is in direct proportion to the density of the air ( $\rho$ ), the rotor sweep area ( $A$ ), the cube of the wind velocity ( $u$ ), and the aerodynamic coefficient ( $C_p$ ) as shown by Equation (1) [25].

$$P = \frac{1}{2} \rho A u^3 C_p \quad (1)$$

The maximum aerodynamic coefficient ( $C_{p_{max}}$ ) for HAWTs can be calculated by the empirical Equation (2), proposed by Wilson et al. [26]:

$$c_{p_{max}} = \left(\frac{16}{27}\right) \lambda \left[ \lambda + \frac{1.32 + \left(\frac{\lambda-8}{20}\right)^2}{B^{2/3}} \right]^{-1} - \frac{0.57 \cdot \lambda^2}{c_D \cdot \left(\lambda + \frac{1}{2B}\right)} \quad (2)$$

where  $\lambda$  is the tip speed ratio (TSR), ranging from 4 to 20,  $B$  is the number of blades, and  $c_L$  and  $c_D$  are the aerodynamic coefficients of lift and drag, respectively. It is apparent that the generated power of HAWTs depends on the airfoils, from which the blades are constructed. Thus, any changes in the flow field could lead to changes in the aerodynamic characteristics of the airfoils, and finally impact the power production of HAWTs.

## 3. Aerodynamic Characteristics of Wind Turbines under Hazard Environmental Conditions

The aerodynamic characteristics of airfoils and wind turbine blades when subjected to adverse environmental conditions necessitates an understanding of how these conditions influence airfoil performance and behavior. Such environmental hazards, such as icing, rainfall, and hailstorms, among others, present specific difficulties that noticeably influence the fundamental principles of airfoil and wind turbine blade aerodynamics.

Icing occurs when supercooled water droplets solidify on the surface of the blade, resulting in an augmented load and structural perturbations that can significantly impair the aerodynamic characteristics of the airfoil. The presence of ice on the surface causes more turbulence in the airflow, leading to increased drag. As a result, the lift generated by the blade decreases, reducing its ability to produce power.

The impact of raindrops on the airfoil surface precipitates an increase in drag and consequent influences on the lift-to-drag ratio, resulting in an overall reduction in operational efficiency and power generation. Moreover, the prolonged interaction of raindrops with the blade's surface can cause erosion, altering the aerodynamic profile and further impinging on the blade's performance.

Hailstorms can cause significant harm as well. When hailstones impact the wind turbine blades, they can cause physical damage to them. This damage includes cracks, dents, and changes in shape, which disrupt the normal airflow, leading to a decrease in performance. The occurrence of hailstorms raises concerns about the safety of both the

wind turbine and its surroundings. To address these concerns, protective measures need to be taken, and strong blade design practices should be implemented.

When dust and sand are carried by the wind, they can potentially abrade the blade surface, inducing alterations in surface smoothness and shape. Furthermore, the accumulation of particles can disturb the airflow over the blade surface, increasing drag and decreasing lift as a result.

Other hazard conditions that degrade the aerodynamic characteristics of HAWTs are insects, humidity, and sea spray. Accumulated insects on blade surfaces block the airflow, causing an increase in drag. Elevated humidity levels influence air density, thus affecting the aerodynamic characteristics of the airfoil. The salty composition of sea spray causes corrosion and material deterioration on blade surfaces, with consequent effects on aerodynamic performance.

To comprehensively examine the various aspects of the aerodynamic characteristics of wind turbines in hazardous environmental conditions, the literature reviewed has been organized into distinct categories. This classification is intended to present readers with a well-structured framework that facilitates their comprehension of the numerous challenges and factors associated with this field. Firstly, the impact of icing on wind turbines' aerodynamic characteristics is thoroughly examined. Then, rainfall, another environmental factor significantly affecting the aerodynamic characteristic of wind turbines, is explored. Following this, hailstorms, known for presenting unique challenges to wind turbines' aerodynamic characteristics and causing damage and performance degradation, are presented. Subsequently, dust and sand are discussed, which are often ignored even though they significantly influence the wind turbines' performance and lifespan. In addition to the previously mentioned categories, additional hazard conditions are addressed, including the effects of insects, humidity, and sea spray, offering a comprehensive perspective on the broader spectrum of environmental challenges.

### 3.1. Icing

Many countries in cold climate regions already harness wind energy and will increasingly rely on it due to their favorable, abundant wind resources. These regions offer a naturally advantageous environment for wind energy utilization. To ensure optimal power production, HAWT manufacturers, including airfoil designers for turbine blades, must account for the challenging conditions caused by atmospheric icing events. Wind farms located in cold regions with higher altitudes are particularly promising, as wind speeds tend to increase by approximately  $0.1 \text{ m}\cdot\text{s}^{-1}$  for every 100 m of altitude over the initial 1000 m [27]. Additionally, colder regions benefit from a wind power potential approximately 10% greater than other areas, thanks to their higher air density. The denser cold air boosts the kinetic energy of the wind, resulting in increased power generation for HAWTs [28]. Figure 2 shows the mean snow cover duration obtained across the last 23 years on an annual basis.

In cold climate regions, icing is a physical phenomenon that significantly impacts the performance of HAWTs and poses a significant challenge. There are two primary types of ice formation: glaze ice and rime ice [21]. Glaze ice forms when rain freezes on cold surfaces and typically occurs near  $0 \text{ }^{\circ}\text{C}$ . It appears transparent and spreads as ice sheets over large areas. On the other hand, rime ice develops when extremely cold moisture droplets in the atmosphere come into contact with a cold surface. Rime ice accumulates in temperatures below  $0 \text{ }^{\circ}\text{C}$ . The presence of ice on aerodynamic surfaces negatively impacts HAWT performance and can lead to sensor failures or inaccurate readings on anemometers and wind vanes. Moreover, ice buildup can lead to rotor imbalances, impaired aerodynamic brakes, and power line disruptions, and pose a risk of falling ice hazards to personnel [21].

The formation of ice on HAWTs (Figure 3) can greatly affect the aerodynamic characteristics and power production. It has been observed that ice growth is influenced by changes in blade design, such as size and airfoil section, as well as the relative velocity

at each section of the blade. Various software codes have been developed to model and predict ice accretion on several surfaces.

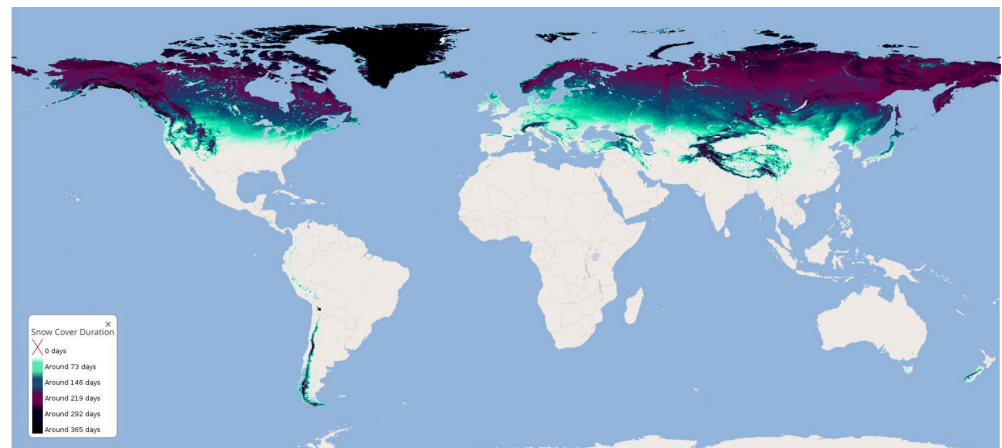


**Figure 2.** Mean global snow cover duration since 1 October 2000 [29].



**Figure 3.** Ice accretion on HAWT blade [30].

- LEWICE is a code for 2D ice accumulation created by the NASA Glenn Research Center [31]. It utilizes a time-stepping procedure to forecast the shape of ice accumulation. The flow field mathematical computations are performed using the Douglas Hess-Smith 2D panel code. The obtained solution is then used to determine particle trajectories and the points at which they impinge on the object. Additionally, LEWICE incorporates an icing model to estimate the rate and shape of ice growth.
- The Turbine Blade Icing Model (TURBICE) is a 2D simulation program specifically designed to anticipate ice accretion on HAWT blades [32,33]. The blade's potential flow field is determined by panel methods, while droplet trajectories and impingement calculations are performed using a Lagrangian technique. Additionally, TURBICE has the ability to estimate the energy necessary for heating in order to prevent ice accumulation on the blade surface.
- FENSAP-ICE represents a premier 3D in-flight icing simulation solver [34,35]. It simulates the flow field, impacts of droplets, and ice shapes, and predicts anti/de-icing heat loads. FENSAP-ICE incorporates integrated computational fluid dynamics (CFD) modules to perform these calculations. The software employs 3D Navier–Stokes

and energy equations to analyze the flow field, along with a 3D Eulerian model for calculating droplet behavior.

Limited efforts have been undertaken to incorporate rotational effects when simulating the 3D model of an entire HAWT blade at full scale [36–38]. The buildup of ice on the blades (Figure 4) affects both the aerodynamic efficiency and safety. Icing can increase blade mass, alter the shape of the aerodynamic profile, cause abnormal tower vibrations, decrease torque, and result in power output losses [39,40]. Even minor icing roughness on the blade surface can lead to a decrease in power output, while a severe icing event has the potential to result in a complete turbine shutdown [41]. Pinar Pérez et al. [42] found that a wind farm consisting of 517 HAWTs experienced a 3% reduction in production as a result of blade icing over a period of 29 months. On the other hand, ice accumulation can lead to an increase in power output by altering the blade profile [41].

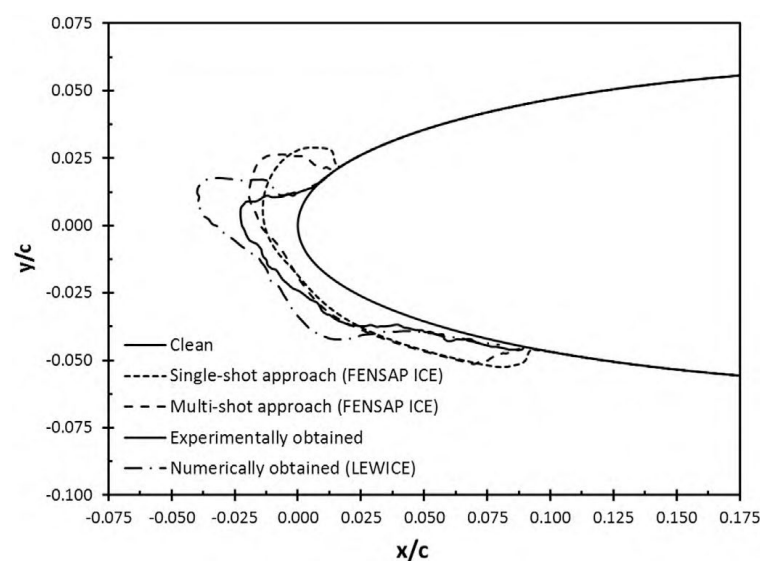


**Figure 4.** Formation of ice on NACA 0012 airfoil, as obtained experimentally and numerically. Reproduced with permission from [43], Elsevier, 2017.

Icing poses a critical challenge for HAWTs operating in cold environments, as it is impacted by multiple fluctuating factors. Ice buildup on the airfoils of turbine blades leads to a significant decline in aerodynamic performance, ultimately leading to a loss in productivity. This ice accretion causes deformation in the airfoil's geometry, leading to pronounced turbulence, especially on the suction side of the airfoil when exposed to high AOAs. Employing modeling and simulation techniques is essential to evaluate the effects of icing on HAWT operations and enhance our comprehension of this phenomenon [44].

During the winter of 1990–1991, Bose [45] closely monitored the natural icing occurrences of a HAWT with a diameter of 1.05 m, designed for battery charging. The most severe icing events were observed as glaze ice accretion, which formed due to freezing rain and drizzle. The icing process exhibited a qualitatively similar pattern at the leading edge (LE) of the blade section, resembling the formation observed on fixed airfoil sections under comparable conditions in icing wind tunnels. The rotational motion of the blades contributed to a greater accumulation of ice at the blade tips compared to the blade roots. While the pressure side of the sections was covered in ice, a significant portion of the suction side remained free of ice.

A large and growing body of literature has investigated the ice formation process on airfoils and HAWT blades [46–52]. The accumulation of ice on HAWT blades is affected by a combination of operating factors such as temperature, velocity, mean volume diameter (MVD), and liquid water content (LWC), as well as geometric characteristics including size

and shape. Varied temperatures and heat distribution across the HAWT blades result in the formation of ice with differing masses and shapes.

Seifert and Richert [53] conducted an experimental investigation on a typical airfoil used in HAWT blades, specifically, the NACA 4415 airfoil. The study examined the aerodynamic coefficients of the airfoil with and without various types of ice formations at the LE. The aerodynamic degradation was more severe when more ice accumulated on the LE. The aerodynamic data obtained from the iced airfoil were utilized as input for load and power calculation codes, and the energy loss was predicted for a typical 300 kW turbine, revealing a 6% to 19% decrease in the AEP, depending on the ice formation, after three months of operation.

Jasinski et al. [54] conducted a study to estimate the impact of rime ice on the performance of HAWTs. They used the NASA LEWICE code to predict four rime ice formations on the S809 airfoil, used for HAWT blade construction, in conditions of usual supercooled fog, prevalent in cold northern regions. Wind tunnel experiments were conducted on the resulting airfoil/ice profiles to analyze the aerodynamic characteristics of lift, drag, and pitching moment at Reynolds numbers ( $Re$ ) ranging from 1 to 2 million. The obtained data were then input into the PROPID HAWT performance prediction software to evaluate the impact of rime ice on a 450 kW rated power, 28.7 m diameter HAWT operating in both stall-regulated and variable-speed/variable-pitch modes. The variable-speed/variable-pitch rotor showed reduced performance of approximately 20%. On the other hand, for the stall-regulated rotor, even a minor rime ice formation led to much greater performance losses.

Hochart et al. [55] experimentally studied the NACA 63 415 airfoil under two in-fog icing conditions. The measurements encompassed the forms and sizes of the ice deposits, alongside the aerodynamic forces exerted on the ice-covered profiles. During the wet-regime testing, glaze primarily developed near the LE and on the pressure side, while also accumulating through run-off on the trailing edge (TE) of the outer portion of the blade. In the dry-regime testing, rime predominantly accreted on the LE forming horn-shaped structures. In both icing events, the presence of glaze or rime on the blade profile resulted in a reduced lift of 40% and an increased drag of about 365% for glaze and 250% for rime ice.

Zhao et al. [56] investigated the fault mechanism of HAWT blade icing through theoretical and experimental analysis. Initially, the aerodynamic characteristics of the S830 airfoil was simulated under normal and icing conditions. The simulation results indicated that the irregular icing coverage significantly alters the airfoil's aerodynamics, leading to a decrease in the lift coefficient and an increase in the drag coefficient, consequently resulting in a direct reduction in power output. Furthermore, icing-induced mass unbalance generated an exciting force causing power frequency vibrations in the HAWT. They concluded that there are two ways to identify icing—through direct and indirect means, with decreases in power output and power frequency vibrations serving as evidence of the presence of icing or similar conditions.

Homola et al. [57] conducted a numerical study to investigate the impact of fluctuations in atmospheric temperature and droplet size on the rate and morphology of ice accretion, as well as the resulting flow field characteristics, for a 5 MW pitch controlled HAWT with blades constructed by the NACA 64-618 airfoil. The findings indicated that while icing leads to a reduction in lift coefficients across all scenarios, the extent of this reduction varied. Specifically, the cases yielding streamlined ice shapes resembling rime ice exhibited minimal changes in lift, whereas those resulting in horn-shaped glazed ice experienced more significant reductions in lift. These results underscore the necessity of obtaining accurate measurements of the atmospheric conditions during icing events to reliably estimate energy production losses, considering the specific shape and type of ice accretion.

Villalpando et al. [58] examined the influence of ice accretion on the aerodynamic coefficients of a HAWT airfoil. CFD simulations were conducted at various AOA, considering both the NACA 63-415 clean airfoil and the same airfoil with ice accumulation. The presence of ice on the airfoil significantly alters the pressure distribution ( $C_p$ ). Notably, it increases the minimum  $C_p$  value, thereby diminishing the suction effect on the suction side

of the airfoil. As pressure forces are the primary contributors to lift and drag coefficients, the aerodynamic characteristics experience notable effects, resulting in reduced lift and increased drag.

Turkia et al. [30] simulated the impact of icing on power output for a typical 3 MW HAWT. Three different rime ice cases were simulated, representing various phases of an icing event: the onset of icing, a brief icing event, and a prolonged icing event. The simulations utilized the in-house code TURBICE to model the accretion of ice masses on HAWT blades. The findings demonstrated that the roughness of the turbine's surface at a small scale had a significant impact on power production. During the initial stages of an icing event, power production was observed to decrease by approximately 17% below rated wind speeds compared to the scenario without ice. With the accumulation of greater ice masses, the reduction in production reached 18% for the short icing event and 24% for the prolonged icing event.

Hudecz et al. [59] conducted experimental and numerical analyses to investigate the impact of glaze, rime, and mixed ice accretion on an NACA 64-618 airfoil at a  $7^\circ$  angle of attack (AOA). The experiments were conducted in a controlled climatic wind tunnel, while the numerical analyses employed the TURBICE ice accretion model. It was observed that the lift coefficient decreased, and the drag coefficient increased as ice accreted. These effects exhibited a nearly linear relationship. Mixed ice formation resulted in the most significant reduction in lift coefficient, while rime ice led to the least reduction. They also concluded that a noticeable decrease in lift and subsequent loss in power production can be experienced within the initial hour of ice accretion.

Hu et al. [60] investigated the ice distribution and load response of various components using the NREL Phase VI HAWT. The study primarily focused on exploring the impact of different parameters on ice distribution, considering the size of dispersed water droplets. The results indicate a linear increase in both ice mass and ice thickness from the root to the tip of the blade. Furthermore, it was observed that both asymmetric icing and symmetric icing lead to a reduction in rotor thrust force, and the blade root moments. In the case of the low-speed shaft, asymmetric icing can introduce an increased imbalance shear force. The resulting asymmetric load can elevate the fatigue damage of the blade by up to 97.6% and that of the tower by up to 70.8%.

Virk et al. [61] simulated the profiles of blade icing for four HAWTs of different sizes. The findings suggest that larger HAWTs experience less severe dry rime icing in terms of both local ice mass and ice thickness. Comparisons between clean and iced profiles revealed noticeable changes in flow behavior and aerodynamic characteristics. Moreover, it was determined that the decrease in torque is more pronounced for the smaller HAWT, providing further evidence to support the hypothesis that dry rime icing has a lesser impact on larger HAWTs compared to smaller ones.

Han et al. [62] conducted CFD simulations, utilizing the dispersed multiphase (DMP) droplet model, to anticipate the development of ice along the LE of a blade tip airfoil. Once verified, their model was utilized to forecast ice formation along the LE of the NACA 64-618 airfoil and predict its aerodynamic behavior under varying environmental conditions. The BLADED software was utilized to conduct steady power computations for the NREL 5 MW HAWT. The modifications in the shape of the airfoil's LE due to ice formation resulted in a 37% reduction in lift coefficient and a 550% increase in drag coefficient. The findings also revealed that the presence of ice on the LE of the blade tip airfoil led to an approximate decrease of 8–29% in HAWT performance.

Ibrahim et al. [43] numerically investigated the forecasting of ice loads on an 80% span HAWT blade section. Simulations of air flow, droplet impingement, and ice accretion using the FENSAP-ICE software were conducted. The analysis focused on assessing the impact of varying low and high LWC conditions on blade thickness. Moreover, it examined all NREL airfoil families commonly utilized in HAWTs to analyze the influence of blade design on ice accretion. The degradation in aerodynamic characteristics resulting from ice formation was

found to be 10–65% in the lift coefficient, a value significantly influenced by the specific shape of the accumulated ice.

Jin and Virk numerically investigated the phenomenon of ice accretion on HAWT blades, focusing on both symmetric and asymmetric airfoils, NACA 0012 and NACA 23012 [63], the DU96-W-180 airfoil [64], and the S826 and S832 airfoils [65]. The findings indicate that the shape and dimensions of the airfoil have a notable influence on the rate and morphology of ice accretion. Specifically, streamlined ice formations were observed on the symmetric airfoil, contrasting with the structures formed on the asymmetric airfoil. In the presence of glaze ice conditions, more complex ice formations can be observed, which have a distinct impact on the aerodynamic characteristics compared to rime ice conditions (Figure 5). The analysis reveals a greater deterioration in aerodynamic characteristics under glaze ice conditions, particularly at higher AOA. Moreover, the S832 airfoil experienced greater changes, particularly under wet ice conditions.

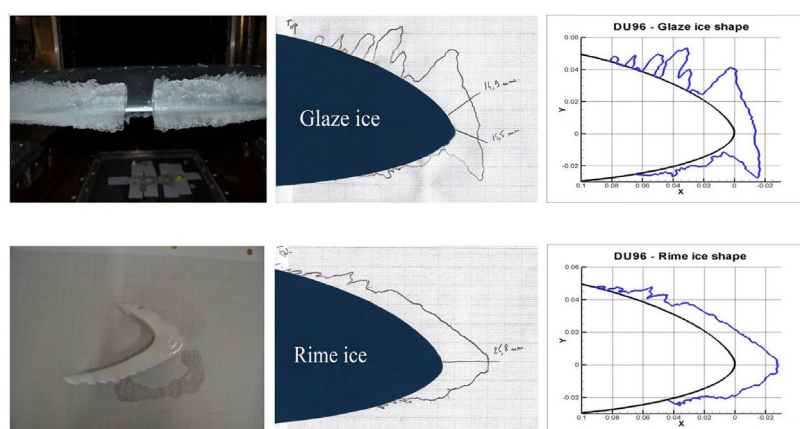


**Figure 5.** Different ice forms obtained experimentally, for glaze and rime ice conditions. Reproduced with permission from [64], Elsevier, 2019.

Yirtici et al. [66,67] developed an ice accretion prediction tool, based on the blade element momentum (BEM) method and the Extended Messenger model, to forecast ice formations on HAWT blades and the resulting power production losses. In their next study [68], they simulated the operation of a 30 kW HAWT in different icing conditions and predicted a power loss of approximately 20% during an hour-long exposure to icing conditions.

Gao et al. [69] experimentally investigated the deterioration of the aerodynamic characteristics of HAWT blades, constructed by the DU91-W2-250 airfoil, caused by the dynamic process of ice accretion. During the ice accretion experiment, it was observed that ice structures formed rapidly on both the upper and lower surfaces of the blade model. These irregular-shaped ice formations significantly disrupted the airflow around the blade, resulting in extensive flow separations and the shedding of unsteady vortex structures from the ice-covered surface. The aerodynamic characteristics of the blade model experienced substantial degradation as a result. The extent of performance deterioration due to ice accretion was found to strongly depend on the AOA of the blade model, with more pronounced degradations occurring at lower AOA. In the case of a  $5.0^\circ$  AOA, the lift force decreased to approximately 12% of its initial value after 10 min of the ice accretion experiment, while the drag force correspondingly increased by a factor of 4.5.

Jiang and Qiu [70] simulated the impact of icing on both the aerodynamic characteristics of the NACA 0012 airfoil and the power efficiency of HAWTs. They found that icing significantly influences the airflow surrounding the airfoil, resulting in the premature appearance of a flow separation vortex. Consequently, the lift coefficient decreases, while the drag coefficient increases. Notably, clear ice exhibits a more detrimental effect on the airfoil compared to frost ice. Furthermore, ice accretion on the airfoil causes a drop in the

power curve, with a stall occurring near the rated wind speed. By analyzing the daily power generation of the HAWT, it was determined that icing results in a power generation loss of up to 4.8%.

Martini et al. [71] studied ice formation on the NACA 64-618 airfoil and estimated aerodynamic losses due to icing. Two turbulence models were used, Spalart–Allmaras and  $k-\omega$  SST, and the impact of surface roughness was also examined. The results matched the experimental data for both clean and iced airfoils, showing increased drag and decreased lift on the iced airfoil. Both turbulence models worked well for the clean airfoil, but the  $k-\omega$  SST model performed better for the iced airfoil. The Spalart–Allmaras model had limitations at high AOAs but was suitable for low angles. Surface roughness significantly affected ice growth and should be considered as a way to estimate the icing effects on aerodynamic characteristics.

Surface roughness on an airfoil can significantly affect ice growth by influencing the interaction between the airfoil's surface and supercooled water droplets. In regions with surface roughness, small-scale irregularities create crevices and protrusions, which promote the formation of ice. This means that in the presence of supercooled water droplets, more ice crystals can start forming on the roughened surface compared to a smooth surface. Moreover, surface roughness can influence the heat transfer rates on the airfoil. Irregularities on the airfoil's surface can lead to variations in temperature, which can affect the rate of ice growth. Specifically, heat transfer rates can be enhanced in areas with roughness, leading to variations in ice accumulation. Furthermore, surface roughness can disrupt the boundary layer flow over the airfoil, resulting in variations in pressure and temperature, which may affect the ice accretion patterns. Disruption of the boundary layer can lead to circumstances favorable for the formation of ice.

Chitransh and Kaur [72] predicted ice formation and acceleration on the NACA 4412 airfoil with the help of a numerical solution. The Extended Messinger method was employed to detect ice deposition, while various parameters relevant to HAWT analysis were also calculated. The simulation reveals that ice deposition on the airfoil has a significant impact on power generation by altering the airfoil's shape. The findings indicate a considerable decrease in the lift coefficient and an increase in the drag coefficient.

Rotich and Kollár [73] examined the influence of ice accretion on the aerodynamic behavior of an NACA 2412 airfoil under various environmental conditions. The lift and drag coefficients for the iced airfoil were calculated, considering different LWCs, AOAs, and accretion times. The results demonstrated that the lift-to-drag ratio is highest shortly after ice begins to accumulate for AOAs up to  $10^\circ$  but significantly decreases with longer accretion times.

Yang et al. [74] analyzed the impact of blade rime icing on a 5 MW offshore floating HAWT with blades constructed using NACA64\_A17, DU21\_A17, and DU25\_A17 airfoils, by using CFD. Results showed concentrated icing on the NACA64\_A17 airfoil's tip. Changes in wind speed had some influence on icing, while temperature had minimal effect. Iced airfoil geometry had little impact on the lift coefficient ( $-34\%$ ) but significantly increased the drag coefficient ( $36\text{--}200\%$ ). Power production decreased by about 17% with iced airfoils compared to clean ones. Table 1 summarizes the different types of airfoils that were examined for icing.

Virk et al. [75] used CFD to analyze ice formation on an NREL 5 MW HAWT blade. Different sections of the blade were tested under various ice conditions and atmospheric temperatures. The results showed that ice formation was milder near the blade root, where the blade chord is larger and thicker. Ice growth varied along the blade, with more ice near the tip. Barber et al. [76] examined, experimentally and computationally, the ice formation effects on HAWT performance. The results show that ice at high altitudes (2330 m) can decrease the power coefficient by up to 22% and AEP by up to 2%, while extreme icing conditions can lead to 17% AEP losses. Icing at the blade tip region (95–100% span) has the strongest impact and icing at high altitudes has less impact than at lower altitudes on AEP.

**Table 1.** Various airfoil types tested in bibliography for icing.

Author	Investigation Method	Airfoil Type	Main Conclusions
Seifert and Richert [53]	experimental	NACA 4415	More ice on the LE led to worse aerodynamic characteristics. AEP dropped by 6% to 19% for a 300 kW turbine.
Jasinski et al. [54]	experimental	S809	The 450 kW rated power rotor with variable speed and pitch had about a 20% decrease in performance.
	numerical		The stall-regulated rotor experienced higher performance losses even with a small amount of ice.
Hochart et al. [55]	experimental	NACA 63-415	Reduced lift by 40% in both icing events. Increased drag by 365% for glaze and 250% for rime ice.
Zhao et al. [56]	theoretical	S830	Icing creates an unbalanced mass, causing vibrations at the power frequency of HAWT.
	experimental		Decreased power output of about 50% and power frequency vibrations are signs of icing.
Homola et al. [57]	numerical	NACA 64-618	Horn-shaped glazed ice led to a more significant reduction in lift than streamlined rime ice. Accurate measurement of atmospheric conditions during icing events is crucial to estimate energy production losses, considering ice shape and type.
Villalpando et al. [58]	numerical	NACA 63-415	The ice on the airfoil increases the minimum pressure coefficient value, reducing the suction effect on the airfoil.
Turkia et al. [30]	numerical	NACA 64-618	In the early stages of ice formation, power production decreased by about 17% below rated wind speed. As more ice accumulated, the reduction increased to 18% for a brief icing event and 24% for a prolonged one.
Hudecz et al. [59]	experimental	NACA 64-618	Mixed ice had the biggest impact on reducing lift, while rime ice had the smallest.
	numerical		Within the first hour of ice formation, there was a noticeable decrease in lift and a loss in power production.
Hu et al. [60]	numerical	S809	Ice mass and thickness increase linearly from the root to the tip of the blade.
			Both asymmetric and symmetric icing reduce rotor thrust force and blade root moments.
			Asymmetric icing on the low-speed shaft can cause an extra shear force imbalance. This asymmetric load can lead to higher levels of blade fatigue damage by up to 97.6% and tower damage by up to 70.8%.
Virk et al. [61]	numerical	NACA 63-215	The decrease in torque is more significant for smaller turbines, supporting the hypothesis that dry rime icing affects them more than larger turbines.
		NACA 63-417	
		NACA 63-416	
Han et al. [62]	numerical	NACA 64-618	The airfoil's shape changed due to ice, causing a 37% decrease in lift and a 550% increase in drag. Ice on the blade tip's LE reduced HAWT performance by about 8–29%.
Ibrahim et al. [43]	numerical	S809	Ice accumulation reduces lift coefficient by 10–65%, depending on the ice shape.

Table 1. Cont.

Author	Investigation Method	Airfoil Type	Main Conclusions
Jin and Virk [63]		NACA 0012	The airfoil's shape and dimensions affect ice formation.
		NACA 23012	For the symmetric airfoil, streamlined ice formations were seen, while the asymmetric one had different structures.
Jin and Virk [64]	numerical	DU96-W-180	Glaze ice led to more complex formations that affected aerodynamic characteristics more than rime ice.
Jin and Virk [65]		S826	Aerodynamic characteristics deteriorated more with glaze ice, especially at higher AOA.
		S832s	The S832 airfoil showed significant changes, especially with wet ice.
Yirtici et al. [66]		NACA 64-618	Icing causes a power loss of 24%.
		S809	
Yirtici et al. [67]	numerical	S809	The estimated quantities of rime and glaze ice, and the maximum ice thickness, exhibit variances ranging from 3% to 25% when compared to experimental data.
		DU93-W210	
Yirtici et al. [68]	numerical	NACA 23012	During exposure to icing conditions for an hour, there is a reduction in power of around 20%.
		NACA 0012	
		DU93-W210	
Gao et al. [69]	experimental	DU91-W2-250	Ice formed quickly on the blade, disrupting airflow and causing flow separations and vortex shedding, negatively affecting the blade's aerodynamic characteristics.
			The degree of degradation depended on the blade's AOA, with greater deterioration at lower angles.
			At a 5.0° AOA, lift force decreased to about 12% of the initial value after 10 min, while drag force increased by a factor of 4.5.
Jiang and Qiu [70]	numerical	NACA 0012	Icing affects airflow around the airfoil, causing flow separation vortex.
			Clear ice is more harmful than frost ice.
			Icing can lead to up to 4.8% power loss in HAWT.
Martini et al. [71]	numerical	NACA 64-618	The airfoil studied is a specific airfoil employed in the blades of the NREL 5 MW reference HAWT.
			Iced airfoils experienced higher drag and lower lift.
			The k- $\omega$ SST model was more effective for the iced airfoil, while the Spalart–Allmaras model had limitations at high AOA but worked well at low angles.
Chitransh and Kaur [72]	numerical	NACA 4412	Surface roughness played a significant role in ice growth and should be considered when estimating the effects of icing on aerodynamic characteristics.
			The presence of ice on the airfoil significantly affects power generation by modifying the shape of the airfoil.
			Considerable reduction in the lift coefficient and an increase in the drag coefficient.
Rotich and Kollár [73]	numerical	NACA 2412	The lift-to-drag ratio reaches its peak shortly after ice accumulation begins for AOA up to 10°.
			The ratio decreases significantly as the accretion time becomes longer.
Yang et al. [74]	numerical	NACA64_A17	Ice concentrated more on NACA64_A17 airfoil's tip.
		DU21_A17	Icing reduced lift coefficient by 34% and increased drag coefficient up to 200%.
		DU25_A17	HAWT power production decreased by 17% with icing.

Homola et al. [77] modeled ice accretion on an NREL 5 MW HAWT blade by using a CFD solver. The calculated power curve changes due to icing were compared with observed differences in power production for an identical turbine operating under icing conditions. The model showed a 27% decrease in power production for wind speeds ranging from  $7 \text{ m}\cdot\text{s}^{-1}$  to  $11 \text{ m}\cdot\text{s}^{-1}$ . These effects were less severe than the observed HAWT, possibly due to a shorter icing event in the model. Their results indicate that modeling can be useful for estimating icing effects and exploring ways to reduce them. In a following study, they suggested [78] that modifying the turbine controller could enhance power production when operating with iced blades.

Dimitrova et al. [79] employed the numerical model PROICET in a HAWT to determine the aerodynamic performance degradation, and the energy and power losses, incurred due to light icing. The findings indicate a general deterioration in aerodynamic characteristics, with lift coefficient losses not surpassing 30% and an increase in the drag coefficient of up to 140%. The aerodynamic performance degradation during light icing precipitation resulted in 3.4% power losses and less than 1% on AEP losses.

In their research, Lamraoui et al. [80] identified the presence of glaze and rime ice on the blade to identify the areas responsible for significant power reduction. The distribution of power production and the characteristics of the accreted ice are inconsistent along the blade. When icing occurs, the aerodynamics of the blade are significantly affected by the outer section of the blade starting at a radial position of  $r/R = 0.8$ . The distribution of the freezing fraction is not uniform; rime ice forms near the root and transitions to glaze ice towards the blade's tip. Their study considers four values of LWC, defining five classes of icing severity, and the major power reduction is found to be situated at  $r/R \sim [0.93 \text{ } 0.96]$  and the maximum power reduction reaches 40%. Regarding power loss, it is observed that, locally, the shape of the ice has a more significant impact than its thickness. However, when considering the entire blade, power degradation is mainly influenced by the ice thickness, irrespective of the ice type.

Etemaddar et al. [81] studied the impact of eight atmospheric and system parameters on the patterns of ice accretion on an NACA 64-618 airfoil, using the 2D ice accumulation software LEWICE 1.6. Among the system parameters, relative wind speed and blade thickness, along with environmental parameters such as LWC and median volume diameter (MVD), are identified as key factors influencing HAWT icing. Through aerodynamic analysis of an iced rotor, it is observed that within the linear region of the lift curve, icing-induced performance degradation primarily stems from an increase in the drag coefficient, as the lift curve undergoes minimal alteration in this particular region. At high AOAs, the discrepancies between the lift coefficients of iced and clean rotors intensify, while the discrepancies in drag coefficients diminish.

Myong [82] employed computational methods to examine the effects of atmospheric icing on the aerodynamics of HAWT blades and also explored the similarities and differences between atmospheric icing on HAWTs and in-flight icing on aircraft. Although certain distinctions exist, such as turbulent shear boundary layers and iced areas other than the LE, many characteristics of aircraft icing can be applied to atmospheric icing on HAWTs. Their findings illustrate that the thickness of ice accumulation increases from the blade root to the tip, and icing conditions, specifically relative wind velocity, significantly influence the shape of the ice buildup. Furthermore, they concluded that ice on the blade surface can cause a substantial reduction in power coefficients across all TSRs.

Reid et al. [83] presented a numerical analysis of the performance degradation of an NREL phase VI rotor operating under icing conditions. By utilizing FENSAP-ICE, simulations were conducted to examine airflow, water impact, and ice accretion. The investigation focused on four different icing conditions, revealing power losses exceeding 60% in certain cases. Simulations with rime ice conditions exhibited lower power losses than those with glaze ice conditions. The glaze ice shape that formed at the largest droplet diameter resulted in the most significant performance degradation, attributed to greater ice thickness and an enlarged contaminated area.

Shu et al. [84] experimentally studied the characteristics and performance of a small HAWT and created a three-dimensional model of a HAWT covered in glaze ice for simulation purposes. An artificial climate chamber was used for the icing experiments, located in Chongqing University, with a 7.8 m diameter and 11.6 m height. The HAWT blade radius was 0.5 m and the chord length ranged from 0.03 m to 0.1 m. The output of the three-phase permanent magnet synchronous motor is 100 W under rated conditions. The findings indicate that the presence of ice considerably diminishes the rotational speed and power output of the turbine. The rate of ice accretion initially increases but then declines over time. Ice accumulates predominantly at the LE, gradually increasing from the root to the tip of the turbine. As the rotational speed decreases, the area covered by ice shifts towards the pressure side. Although a higher wind velocity and lower temperature deteriorate the impact of ice, they do not alter its shape. Ice load seems to have a larger effect on the performance of the rotor in small HAWTs compared to the degradation of aerodynamic characteristics.

The same researchers [85] conducted a study focusing on the ice formation on HAWT blades and its impact on the power performance of a 300 kW HAWT operating in a natural icing environment (Figures 6 and 7). The results indicated a significant decrease in power output at higher wind speeds following blade icing, with the severity of deterioration increasing as the ice thickness at the blade tip grows. Furthermore, it was observed that irregular and coarse ice formations have a more detrimental effect on power performance. The rotor speed of iced rotors noticeably decreases at the same wind speed as the ice thickness increases. In icing cases, both the power and moment coefficients experience a greater decline as the ice thickness increases, at the same TSR. Additionally, the maximum power and moment coefficients in icing cases occur at lower TSRs. Later, they proposed a 3D numerical simulation model to assess blade aerodynamics after icing, by employing the multiple reference frame model, Reynolds-Averaged Navier–Stokes (RANS), and the  $k-\omega$  SST turbulence model [86]. The results demonstrate agreement between computational and experimental clean and rime-iced rotors within rated wind speed, but overestimation for glaze-iced rotors at high wind speed. Increasing the wind speed leads to significant decreases in rotor speed and power output under icing conditions. Ice shapes primarily impact pressure distribution at the airfoil's LE, reducing normal and tangential forces, and result in stall at the same wind speed and heightened flow separation, particularly for glaze ice.

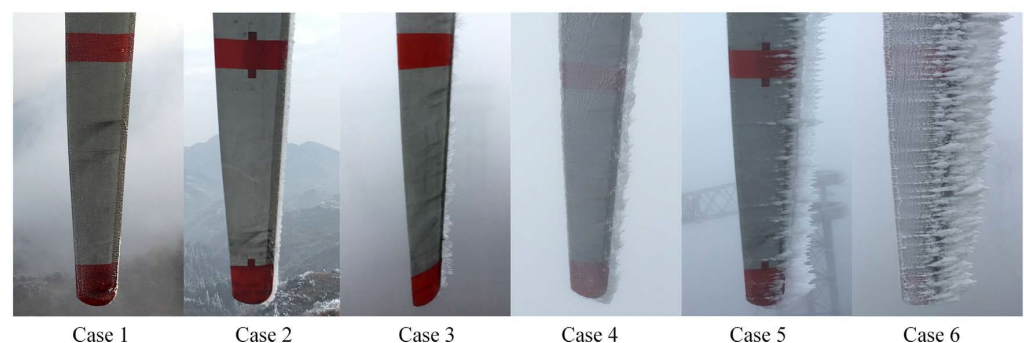


**Figure 6.** Photos of ice accretion on blade tip under various icing conditions, from light icing (case 1) to severe icing (case 6). Reproduced with permission from [85], Elsevier, 2018.

Zanon et al. [87] introduced a numerical methodology that effectively simulated the transient occurrence of ice accretion and its consequences on the performance of HAWTs. The NREL 5 MW reference HAWT was utilized to apply this approach, aiming to forecast its performance throughout and following an 8 h period of icing, and the potential enhancement in energy extraction through various operational strategies. The findings indicate that by reducing the rotational speed of the turbine and accepting a minor decline in energy conversion during the icing event, the performance can improve by up to 6% once

full operation is restored, in comparison to the baseline operational strategy. Conversely, maintaining the rotational speed during the icing event can result in a subsequent 3% decrease in performance, relative to the same baseline.

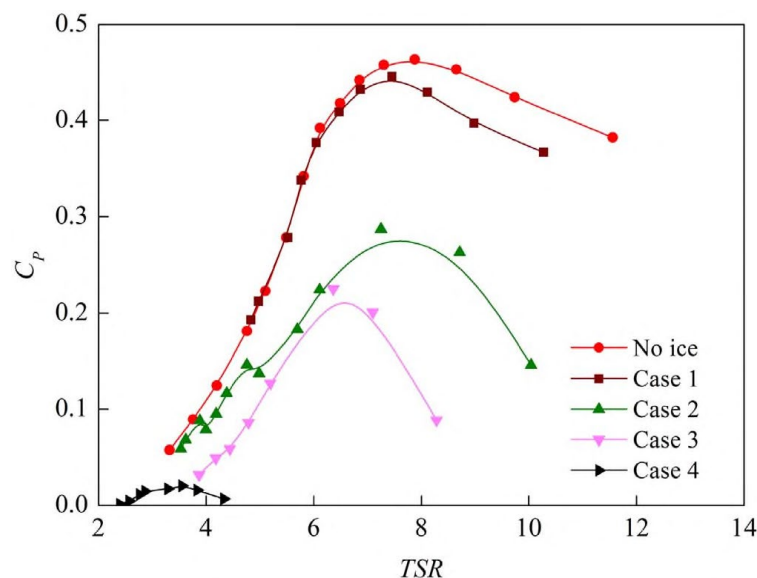


**Figure 7.** HAWT power coefficient versus TSR at various icing conditions, from light icing (case 1) to more severe icing (case 4). Reproduced with permission from [85], Elsevier, 2018.

Tabatabaei et al. [88] evaluated the accuracy and limitations of the BEM method in icing conditions. They investigated the aerodynamic performance of the full-scale NREL 5 MW rotor through computational simulations. Three-dimensional steady RANS simulations were employed to analyze both clean and iced blades, while 2D CFD airfoil data were used for BEM calculations. The calculated total power using the BEM method closely aligns with the 3D CFD results for the clean blade, with a deviation of 4%. However, for the iced blade, the BEM method underestimates the total power by 28%. The way the load is distributed along the span of the clean blade varies between the two methods. The 3D CFD predicts a 32% load loss in extracted power due to the presence of ice, with the main loss occurring in areas where the height of the ice horn is greater than 8% of the chord length.

Caccia and Guardone [89] conducted a simulation to analyze ice accretion on the NREL 5 MW HAWT blade, utilizing the BEM approach. To enhance accuracy in calculating ice shapes, they proposed utilizing independent time steps in a multi-step ice accretion simulation. Additionally, they investigated the impact of surface roughness on the aerodynamic characteristics of the iced sections, by considering two roughness extensions and two roughness heights for each section. By calculating the aerodynamic coefficients for each case, they evaluated whether the observed aerodynamic penalty resulted from ice, roughness, or both. The findings demonstrated that even in the presence of a complex ice shape, roughness can significantly influence the aerodynamics of an iced section when the roughness height is sufficiently significant. The extended roughness case that was studied assumed a roughness height of  $k_s/c = 3 \times 10^{-3}$  and an extended roughness region covering 25% of chord length, specifically 0.44 m, on both airfoil surfaces and on all sections along the blade. That high-roughness case exhibited a power loss that was 50% greater than the low-roughness case.

Yirtici and Tuncer [90] conducted an aerodynamic shape optimization study conducted to minimize power production losses caused by ice on HAWT blades. Their study focused on the Aeolos-H 30 kW HAWT exposed to icing conditions for 30 min at a wind speed of 11 m/s. Through optimization, the power losses due to icing were reduced by approximately 4%. Similarly, for the larger NREL 5 MW HAWT, the optimized blade design reduced the power losses by about 1%. The study concludes that optimizing blade profiles

around the LE is most efficient for low Re and small-scale HAWTs. Table 2 provides a summary of various types of HAWTs that underwent examination regarding icing.

**Table 2.** Various HAWT types tested in bibliography for icing.

Author	Investigation Method	HAWT	Main Conclusions
Virk et al. [75]	numerical	NREL 5 MW	Ice formation exhibited lower severity close to the blade root. The growth of ice varied along the blade, with a greater presence of ice observed towards the tip.
Barber et al. [76]	experimental	ETH Zurich subscale model	Ice reduces power coefficient by up to 22% and AEP by up to 17% for severe icing.
	numerical		Blade tip icing has the greatest impact, while high-altitude icing has less impact than lower-altitude icing on AEP.
Homola et al. [77]	numerical	NREL 5 MW	A 27% decrease in power production for wind speeds 7–11 m/s. Modeling can help estimate icing effects and find ways to reduce them.
Homola et al. [78]	numerical	NREL 5 MW	Reduction in power production by 27% for wind speeds ranging from 7 m/s to 11 m/s, Adjusting the turbine controller can improve power production with iced blades.
Dimitrova et al. [79]	numerical	Vestas V80 1.8 MW	Aerodynamic characteristics decline with light icing, causing up to 30% loss in lift coefficient and a maximum increase of 140% in drag coefficient.
			This leads to a 3.4% power loss and <1% decrease in AEP.
Lamraoui et al. [80]	numerical	Vestas V80 1.8 MW	Both glaze and rime ice on the blade affect power. Outer section from $r/R = 0.8$ significantly affects aerodynamics.
			Freezing fraction is non-uniform, with rime ice close to the root and glaze ice towards the tip.
			Major power reduction occurs around $r/R \sim [0.93 \ 0.96]$ with a maximum reduction of 40%. Ice shape has a bigger local impact than thickness, but blade-wide, thickness matters most for power loss, regardless of ice type.
Etemaddar et al. [81]	numerical	NREL 5 MW	In the linear region of the lift curve, ice-induced performance degradation mainly occurs due to higher drag coefficient. At high AOAs, the differences between the lift coefficients of iced and clean rotors become more pronounced, while the differences in drag coefficients decrease.
			During icing, nearly 50% less power is produced at cut-in wind speed, and as wind speed increases, the difference diminishes.
Myong [82]	numerical	NREL 5 MW	Many aircraft icing features can be applied to icing on HAWTs. Ice thickness grows from the base to the tip of the blade. Ice on the blade reduces power coefficients at all tip speeds.
Reid et al. [83]	numerical	NREL phase VI	Some icing conditions showed power losses over 60%. Simulations with rime ice had less power losses than glaze ice.
			Glaze ice at the largest droplet size caused the greatest performance decline due to thicker ice and a larger contaminated area.
Shu et al. [84]	experimental	Small HAWT (with blade radius 0.5 m)	The presence of ice slows down the turbine and reduces its power. Ice builds up more at the front edge and increases from the base to the tip of the turbine.
			As the speed decreases, the ice shifts to the other side.
			Higher wind and lower temperature make ice less effective but do not change its shape.
			Ice load affects small HAWTs more than changes in aerodynamics.

Table 2. Cont.

Author	Investigation Method	HAWT	Main Conclusions
Shu et al. [85]	experimental	300 kW HAWT (with blade radius 14.6 m)	Power output decreases as wind speed increases and ice thickness at the blade tip grows.
			Irregular and coarse ice formations have a more negative impact on power performance.
			Iced rotors experience a noticeable decrease in rotor speed as ice thickness increases.
			In icing conditions, power and moment coefficients decline more as ice thickness increases, at the same TSR.
			Maximum power and moment coefficients in icing conditions occur at lower TSRs.
Shu et al. [86]	numerical	300 kW HAWT (with blade radius 14.6 m)	An hour of icing leads to a power loss of approximately 31.8% for wind speeds 6–7 m/s.
			Computational and experimental results show agreement for clean and rime-iced rotors at rated wind speed, but overestimate for glaze-iced rotors at high wind speed.
			Higher wind speed reduces rotor speed and power output when icing occurs.
Zanon et al. [87]	numerical	NREL 5 MW	Ice shapes primarily impact pressure distribution at the airfoil's front edge, decreasing normal and tangential forces, causing stall at the same wind speed and increased flow separation, especially with glaze ice.
			By lowering the turbine's rotational speed during icing, the performance can increase by up to 6% once normal operation resumes.
Tabatabaei et al. [88]	numerical	NREL 5 MW	Maintaining the speed during icing can lead to a 3% decrease in performance compared to the baseline.
			The BEM method agrees closely with the 3D CFD results for the clean blade (4% deviation) but underestimates the total power for the iced blade by 28%.
Caccia and Guardone [89]	numerical	NREL 5 MW	The 3D CFD predicts a 32% loss in extracted power due to ice, mainly when the ice horn height is over 8% of the chord length.
			When the ice shape is complex, roughness can greatly affect the aerodynamics of an iced area if the roughness is significant enough.
Yirtici and Tuncer [90]	numerical	Aeolos-H NREL 5 MW	In the high-roughness case, there was a 50% higher power loss compared to the low-roughness case.
			The optimization of HAWT blades reduced losses by about 4% for Aeolos-H turbine and 1% for NREL 5 MW.

### 3.2. Rainfall

Among the various meteorological conditions during HAWT operation that can impact their performance is rainfall, which leads to a decrease in aerodynamic lift and an increase in drag [91–93]. Moreover, the low-pressure region above the airfoil experiences significant water vapor condensation, releasing latent heat from water droplets [93]. The remaining raindrops form a thin water film on the airfoil surface, which is subsequently affected by subsequent raindrops. This interaction results in the formation of craters and an uneven film, effectively roughening the airfoil surface and causing increased drag [94].

Figure 8 shows the average precipitation globally, and it is evident that there is a necessity to study the operation of HAWTs under rainfall and hailstorm conditions. Limited investigation has taken place regarding the impact of rain on the operational efficiency of HAWTs, despite rain being a frequent occurrence in certain regions. While numerous studies have explored the effects of rain in aviation applications [95–103], similar investigations specifically focused on HAWTs remain scarce. Research from the airfoil and aircraft industry highlights the adverse impact of rain on drag and lift, causing a significant reduction in power generation. Consequently, there is an evident necessity for a

comprehensive examination of HAWT performance in rainy conditions and the subsequent reduction in operational efficiency.

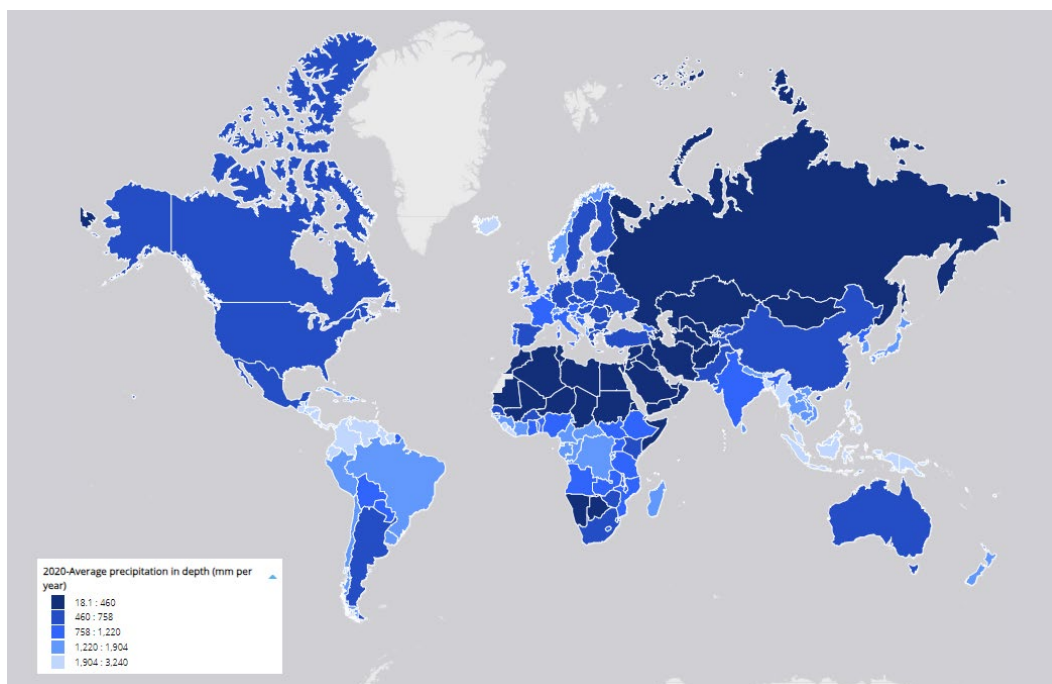


**Figure 8.** Average precipitation in 2020 globally. Precipitation is the water that falls from clouds in either liquid or solid form [104].

The first systematic research about the effects of precipitation on HAWT power output was conducted by Corrigan and Demiglio [105]. They experimentally studied the two-bladed Mod-0 HAWT with three different rotor configurations and revealed the impact of rain on its performance. The results indicated a degradation in performance due to rain, with light rainfall leading to a decrease of up to 20% and heavy rainfall up to 30%. Furthermore, when snow was mixed with drizzle, the performance degradation reached as high as 36% in low wind speeds. Additionally, an analysis was performed to forecast the impact of rain on HAWT performance. Their analysis utilized a BEM code, incorporating adjusted airfoil characteristics to account for the rain effect. The analysis predicted a performance loss of 31% in high winds with moderate rainfall rates, and these projected results corresponded well with the experimental data.

CFD advancements over the past decades have contributed significantly to enhancing our understanding of the dynamics of two-phase flows. Rainfall can be characterized as a two-phase flow, necessitating the utilization of CFD codes to address supplementary transport equations for the second phase. Moreover, these codes facilitate the management of interaction terms encompassing mass, momentum, and energy exchanges between the phases. In the modeling of fluid–particle flows, two prevalent approaches have been extensively examined by researchers such as Valentine and Decker [106], as well as Durst et al. [107].

Following these, Luers [108] analyzed, theoretically, the aerodynamic performance of the same HAWT, and the computational results aligned well with the experimental data from Corrigan and Demiglio [105]. According to Luers' [108] findings, there is a significant 25% power loss at a wind speed of 10 m/s and a rain rate of 50 mm/h. Additionally, notable performance penalties are observed even under less intense rain conditions and lower wind speeds. It has been determined that the deterioration in performance is attributed to the aerodynamic roughness caused by the impact of raindrops and the waviness of the water film on the HAWT's blades.

Cai et al. [109] developed a novel CFD model to evaluate the performance of the S809 airfoil under rainy conditions. These validated single-phase simulation results served

as a reference point for quantifying the impact of rain on the HAWT's performance. By employing a coupled Lagrangian–Eulerian approach, they captured the formation of a water film over the airfoil. Through the accurate representation of the water film's shape and position, they estimated the resulting performance loss, and they concluded that heavy rain could lead to considerable performance degradation of the airfoil.

Douvi and Margaris [110] simulated the heavy rain over the NACA 0012 airfoil by employing the Discrete Phase Model (DPM) and computed lift and drag coefficients at various AOs under both dry and wet conditions. The findings indicated that heavy rain significantly affects airfoil performance, leading to a decrease in lift and an increase in drag. The degradation is a result of water film formation on the airfoil's surface and the impact-induced cratering from raindrops. The rate of degradation is more pronounced at higher AOs. The computational results also reveal droplet breakup near regions with severe pressure gradients, forming an “ejecta fog” near the airfoil and causing water streams to flow from the TE.

Douvi et al. [92,94] studied, experimentally and computationally, the influence of different rainfall rates on the aerodynamic characteristics of the NACA 0012 airfoil operating at a low Re. To simulate various rainfall rates, they injected water droplets upstream of the airfoil model using commercial rain simulation nozzles, achieving four different LWCs, and they used a CFD code to gain further insight into the flow field. Their findings indicated that as LWC increased, the degradation of aerodynamic characteristics also increased, particularly up to the stall angle. Additionally, stall onset was delayed for all rainfall rates. The computational results revealed that larger droplets were more prone to droplet breakup, particularly in regions with severe pressure gradients near the airfoil (Figure 9). The thickness of the water film on the upper surface of the airfoil increased with higher LWC. The maximum height of the water film appeared near the TE at a  $0^\circ$  AOA for all LWCs but shifted towards the LE at higher AOs. Furthermore, as the AOA increased, less water accumulated on the upper surface of the airfoil for all LWCs. Finally, they observed that the rivulet formation point on the upper surface of the airfoil was close to the TE for low AOs and moved towards the LE with increasing AOA.

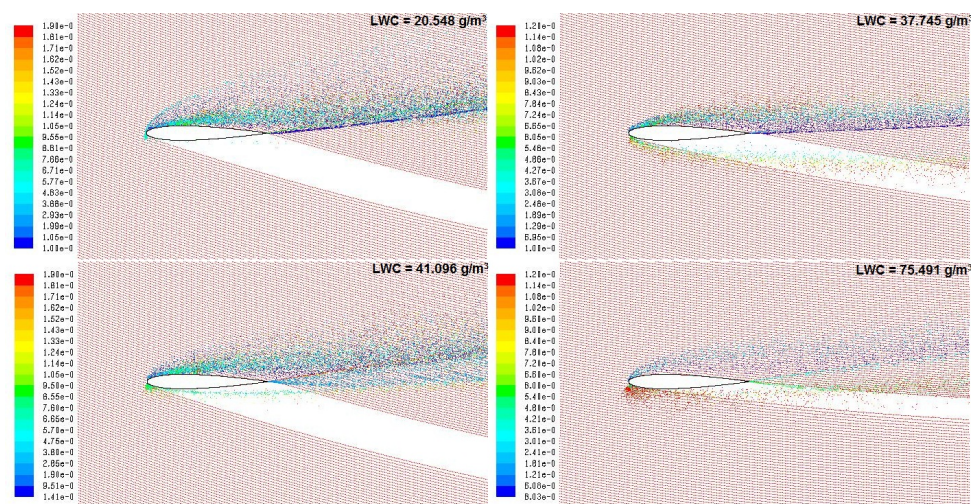


**Figure 9.** Droplets' diameter over NACA 0012 airfoil at a  $9^\circ$  AOA, under varying LWCs [92].

Cohan and Arastoopour [111] enhanced the Cai et al. [109] model and developed a CFD model to investigate the influence of rainfall rate, surface tension, and surface properties on HAWT blades by employing the DPM and the Eulerian Volume of Fluid (VOF) model. They noticed that, at low rainfall rates, the airfoil's performance is highly responsive to the rainfall rate. However, when the rainfall rate becomes sufficient to form water film on the airfoil surface, further increases in rainfall do not substantially impact its

performance. At higher rainfall rates, the lift coefficient is higher compared to the no-rain case but accompanied by an unfavorable increase in the drag coefficient.

Arastoopour and Cohan [112] refined their previous CFD model [111] to more effectively simulate the transfer of momentum during the formation of water films on the airfoils of a HAWT. The 2D airfoil simulation demonstrated an increase in the lift coefficient with the AOA, surpassing the stall angle observed in the single-phase case. However, this favorable lift increase was accompanied by a higher drag coefficient, particularly at larger AOAs. Furthermore, they examined the impact of rainwater films on the turbine performance using the 3D NREL Phase VI HAWT as a case model and concluded that the accumulation and flow of rain film on the turbine airfoil surface led to a reduction in power output by up to 25% at a wind speed of 7 m/s and a rainfall rate of 40 mm/h.

Wu et al. [113,114] presented a hybrid method designed to analyze the dynamic characteristics of HAWTs operating under wind–rain conditions, which utilizes a Eulerian multiphase model to represent the flow of wind and rain, a single rotating frame to simulate the rotational motion of HAWTs, and collision theory to calculate the load generated by rain. Numerical simulations were conducted to investigate various scenarios involving wind speed, rotation speed, and rain intensity for a 5 MW HAWT. The results clearly indicate that the impact of rain on the HAWT is more pronounced near the blade tip during rotation, whereas free-falling rain primarily affects the region near the blade root. Moreover, the rain-induced load, in terms of thrust and torque, increases with higher rain intensity. Additionally, empirical formulae are derived from the numerical results to describe the relationship among the three influencing factors, i.e., wind speed, rotation speed, and rain intensity, and the rain-induced load coefficient.

Barfknecht et al. [18] calculated and compared the AEP loss resulting from LE erosion (LEE) and from operating in an Erosion-Safe Mode (ESM) for the IEA 15 MW and NREL 5 MW offshore HAWTs. Performance evaluations were conducted under uniform and sheared inflow conditions for both turbines, with a focus on identifying trends and trade-offs between LEE and the ESM. LEE negatively impacts power production below rated capacity, while operating in the ESM predominantly reduces performance at the turbine's rated power. The IEA 15 MW reference turbine experienced a higher performance loss due to erosion, particularly at lower wind speeds, compared to the NREL 5 MW turbine. However, the turbine design had little sensitivity to the break-even point for the ESM.

Anh and Duc [115] presented an analytical method and model that simulated the physical processes of raindrops forming on the blades of HAWTs. Their model estimated the effect of precipitation, determined optimal wetness, and subsequently evaluated power and performance, under various rainy weather conditions, considering different turbine blade geometrical shapes. They found that the wetness on HAWT blades corresponded to the impact force of rain, with an optimal wind speed minimizing both the impact force and power loss. Moreover, larger raindrop size significantly reduced power output, affecting the rotation speed of HAWT blades. In a following study, Anh and Duc [116] proposed an analytical method to study the power output of a HAWT and the operation of the pitch control system under various rainy conditions. Their model simulated the physics-based process of raindrops falling on the blades' surfaces, enabling the determination of optimal wetness levels based on the swept area's shape. Subsequently, they analyzed the power generation and performance of the HAWT in rainy conditions, and the results indicated that during rain, the pitch angles should be decreased when the wind speed exceeds the predefined threshold value.

Douvi et al. [117] investigated the aerodynamic characteristics of HAWT with three blades, constructed by NACA 4418 airfoil, under three different rainy conditions. The blade geometry was optimized using the TTbEM application [118], while a commercial CFD code was employed for simulations. The study first analyzed the blade's operation in dry conditions and subsequently examined different rainfall scenarios to evaluate rain droplets' impact on the turbine's aerodynamic performance. It concluded that rain negatively affects the aerodynamic performance of the HAWT, specifically causing a decrease in the power

coefficient as the LWC and droplet diameter increase. A significant decline in aerodynamic efficiency compared to the single-phase flow was observed: reductions of 11.84%, 16.87%, and 23.9% were identified for rain densities of  $10 \text{ g/m}^3$ ,  $30 \text{ g/m}^3$ , and  $60 \text{ g/m}^3$ , respectively. Notably, the maximum water film thickness was observed near the hub, where the blade's chord length is greater, while a smaller amount of water accumulated near the blade tip due to centrifugal force removing the water from the blade. Additionally, under a two-phase flow with an LWC of  $30 \text{ g/m}^3$ , power coefficient reductions of 15.33%, 16.87%, and 17.99% were observed for raindrop diameters of 0.5 mm, 1 mm, and 2 mm, respectively. Table 3 shows the different types of airfoils and HAWTs that have been tested in the literature for rainfall.

**Table 3.** Various airfoil and HAWT types tested in bibliography for rainfall.

Author	Investigation Method	HAWT or Airfoil Type	Main Conclusions
Corrigan and Demiglio [105]	experimental	two-bladed Mod-0 HAWT	Light rainfall caused up to a 20% decrease, while heavy rainfall caused up to a 30% decrease in aerodynamic performance.
			When snow mixed with drizzle, performance dropped by as much as 36% in low winds.
			A 31% performance loss occurs in high winds with moderate rainfall, which aligned with the experimental data.
Luers [108]	theoretical	two-bladed Mod-0 HAWT	A 25% power loss occurs at a wind speed of 10 m/s and a rain rate of 50 mm/h.
			Even under lighter rain and lower wind speeds, noticeable performance issues are seen.
			The decrease in performance is due to the roughness caused by raindrops and the waviness of the water film on the HAWT's blades.
Cai et al. [109]	numerical	S809 airfoil	They observed water forming on the airfoil and estimated how it affected performance. Heavy rain can significantly degrade the airfoil's performance.
Douvi and Margaris [110]	numerical	NACA 0012 airfoil	Heavy rain affects airfoil performance, reducing lift and increasing drag, due to water film formation on the airfoil's surface and impact-induced cratering from raindrops.
			The degradation is more significant at higher AOA.
			Droplets break up near areas with severe pressure gradients, creating an "ejecta fog" near the airfoil and causing water streams to flow from the TE.
Douvi et al. [92,94]	numerical	NACA 0012 airfoil	Increasing LWC degrades aerodynamic characteristics, especially up to stall angle.
			Rainfall delays stall onset. Larger droplets break up more in areas with pressure gradients near the airfoil.
			Higher LWC increases water film thickness on the upper airfoil surface.
			The maximum water film height near TE occurs at $0^\circ$ angle, shifting towards LE at higher angles.
			With higher AOA, less water accumulates on the upper surface.
Rivulet formation point on upper surface moves from TE to LE with increasing AOA.			
Cohan and Arastoopour [111]	numerical	S809 airfoil	At low rainfall rates, the airfoil's performance is affected by rainfall.
			When the rainfall rate is enough to form a water film on the airfoil surface, further increases in rainfall do not significantly affect performance.
			Higher rainfall rates increase the lift coefficient, but are also detrimental to the drag coefficient.

Table 3. Cont.

Author	Investigation Method	HAWT or Airfoil Type	Main Conclusions
Arastoopour and Cohan [112]	numerical	S809 airfoil	Increasing the AOA in the airfoil simulation increased the lift coefficient but also resulted in a higher drag coefficient.
		NREL Phase VI HAWT	Rain film accumulation and flow on the airfoil surface reduced power output by up to 25% at a wind speed of 7 m/s and a rainfall rate of 40 mm/h.
Wu et al. [113,114]	numerical	NREL 5 MW	The results show that rain affects the HAWT differently at the blade tip and root.
			Rain intensity increases the impact.
Barfknecht et al. [18]	numerical	IEA 15 MW and NREL 5 MW offshore HAWTs	Empirical formulae describe the relationship between wind speed, rotation speed, rain intensity, and the load caused by rain.
			The IEA 15 MW turbine had higher erosion-related performance loss at lower wind speeds compared to the NREL 5 MW turbine.
Anh and Duc [115]	numerical	---	Turbine design had little sensitivity to the Erosion-Safe Mode break-even point.
			The wetness on turbine blades correlates with the impact force of rain.
Anh and Duc [116]	numerical	---	The optimum wind speed reduces both the impact force and power loss.
			Larger raindrops lower power output and affect blade rotation.
Anh and Duc [116]	numerical	---	Optimal wetness levels based on the blade shape were determined.
			Pitch angles should decrease when wind speed exceeds a set threshold during rain.
Douvi et al. [117]	numerical	Optimized three-bladed HAWT, with blades constructed by NACA 4418 airfoil	The power output reduced under rainfall of about 7%, for wind speeds 8–12 m/s.
			Rain has a detrimental impact on HAWT aerodynamics, causing a decrease in power coefficient as raindrop size and LWC increase.
Douvi et al. [117]	numerical	Optimized three-bladed HAWT, with blades constructed by NACA 4418 airfoil	Significant reductions in aerodynamic efficiency were observed, with declines of 11.84%, 16.87%, and 23.9% for rain densities of 10 g/m <sup>3</sup> , 30 g/m <sup>3</sup> , and 60 g/m <sup>3</sup> , respectively.
			The thickest water film accumulated near the hub, where the blade chord is longest, while less water collected near the blade tip due to centrifugal force.
Douvi et al. [117]	numerical	Optimized three-bladed HAWT, with blades constructed by NACA 4418 airfoil	Under rainfall with an LWC of 30 g/m <sup>3</sup> , power coefficient reductions of 15.33%, 16.87%, and 17.99% occurred for raindrop diameters of 0.5 mm, 1 mm, and 2 mm, respectively.

### 3.3. Hailstorms

Hailstorms are less frequent than rainfalls, but they can cause significant damages to infrastructures, resulting in financial and insured damages [119]. Unlike rain, the solid particles that prevail in hailstorms include a wide range of shapes and sizes. Hailstones, for instance, are larger than 5 mm, and no upper limit exists; some of the largest hailstones ever recorded reached a diameter of approximately 20 cm [120]. In the Midwest of the USA, where numerous HAWTs operate, hail is a common phenomenon [121]. However, there is a lack of similar data on hail events in the North Sea region. Europe, on the other hand, experiences fewer hail occurrences when compared to the USA, although they constitute a significant meteorological risk as well [119].

Fiore et al. [122] investigated, numerically, the damage caused by raindrops and hailstones over a HAWT blade. The trajectory of the particles hitting the blades was analyzed using a numerical code, the areas of the blade surface that were subjected to damage were estimated, and it was found that they depend on the airfoil type, the AOA, and the particle mass. More raindrops and hailstones were captured by the blade section constructed by thinner airfoils. Notably, the hailstones generated significant impact forces

at the LE of the blade due to the angle of their trajectory in relation to the blade surface. On the other hand, raindrops are more sensitive to the flow field around the blade compared to hailstones. This sensitivity is reflected in the impact force's dependence on the blade's AOA. The erosion rate resulting from raindrop impact is found to be proportional to the cube of the blade's relative wind velocity, while the impact force exhibits a power-law relationship with the square of the wind velocity.

Douvi et al. examined, computationally, the impact of hailstorm conditions on the aerodynamic characteristics of the S809 [123] and the NACA 0012 [124] airfoils. The results confirmed that hailstorm conditions have a significant effect on the aerodynamic characteristics of both airfoils, resulting in a decrease in the lift coefficient and an increase in the drag coefficient when compared to normal airflow. When operating under hailstorm conditions, discrepancies between the hailstorm and air flow contours were observed primarily at the TE and LE of the airfoils. Furthermore, the analysis of hailstone and water droplet distribution around the airfoils revealed that both particles impact the airfoils, breaking up into smaller particles. Shadow zones were also apparent, and it was concluded that an increased AOA leads to a wider distribution of smaller hailstones across the upper surface of the airfoil and a higher concentration of hailstones below the airfoil. Ultimately, the prediction of the power coefficient for a three-bladed HAWT indicated a decrease in power coefficient during hailstorm conditions.

Douvi and Douvi [125] expanded their research to study the pressure coefficient and wall film height, both on the upper and lower surfaces of the S809 airfoil, while operating in hailstorm conditions. A significant finding of this study was that the upper surface of the airfoil near the LE displayed the highest wall film height for all AOAs. These findings support the notion that particles contribute to the deterioration of airfoil aerodynamics due to the roughness of the LE. The wavy nature of these curves reflected the shape of the water film on the airfoils. Increasing the AOA resulted in reduced water accumulation on the upper surface and increased water presence on the lower surface of the airfoil. Lastly, the prediction of the power coefficient for a three-bladed HAWT using the S809 airfoil profile indicated a decrease in the power coefficient during hailstorm conditions for various TSRs, ranging from 0.87% to 1.35% for TSRs ranging from 5 to 8.

Douvi et al. [126] conducted a novel computational study investigating the aerodynamic performance of an optimal three-bladed HAWT during hailstorm conditions when hailstones and raindrops are present. This study explored not only the power output of a HAWT operating under hailstorm conditions but also comprehensively analyzed the entire flow field, providing valuable information about the regions on the blade susceptible to erosion and offering insights into the wake development downwind of the HAWT rotor (Figure 10). The findings indicate that the HAWT's aerodynamic performance declines due to particle impact and breakup on the blade. Table 4 provides several airfoils and HAWT types studied in the literature for operating under hailstorm conditions.

**Table 4.** Various airfoil and HAWT types tested in bibliography for hailstorm conditions.

Author	Investigation Method	HAWT or Airfoil Type	Main Conclusions
Fiore et al. [122]	numerical	DU 97-W-300 airfoil	Thinner airfoil sections captured more raindrops and hailstones.
		DU 96-W-212 airfoil	Hailstones generated significant impact forces at the blade's LE due to their trajectory angle.
		DU 96-W-180 airfoil	Raindrops were more influenced by the blade's flow field and AOA, affecting their impact force.
			Raindrop erosion rate correlated with the cube of the blade's relative wind velocity, while impact force followed a power-law relationship with wind velocity squared.
Douvi et al. [123]	numerical	S809 airfoil	Hailstorms significantly affect airfoil aerodynamics, leading to decreased lift coefficients (up to 2.3%) and increased drag coefficients (up to 7.7%) compared to normal airflow. These effects were particularly notable at the airfoil's TE and LE.

Table 4. Cont.

Author	Investigation Method	HAWT or Airfoil Type	Main Conclusions
Douvi et al. [124]	numerical	NACA 0012 airfoil	<p>Hailstones and water droplets impacting the airfoils fragmented into smaller particles, and shadow zones were observed.</p> <p>Increasing the AOA resulted in a wider distribution of smaller hailstones on the airfoil's upper surface and a higher concentration on the lower surface.</p> <p>The power coefficient prediction for a three-bladed HAWT indicated a decrease during hailstorm conditions.</p>
Douvi and Douvi [125]	numerical	S809 airfoil	<p>The airfoil's upper surface near the LE consistently had the highest wall film height, suggesting that particle accumulation contributes to airfoil aerodynamic deterioration, especially at the LE.</p> <p>The shape of wall film curves implies the water film's wavy shape on the airfoils.</p> <p>Increasing the AOA led to reduced water accumulation on the upper surface and more on the lower surface of the airfoil.</p> <p>Decrease in power coefficient of a three-bladed HAWT using the S809 airfoil profile during hailstorm conditions, ranging from 0.87% to 1.35%, across different TSRs.</p>
Douvi et al. [126]	numerical	Optimized three-bladed HAWT with blades constructed by S809 airfoil	<p>The turbine's power decreases by 6.4% at a wind speed of 10 m/s and by 3.0% at 15 m/s under hailstorm conditions.</p> <p>Hailstorms create rings of varying speeds and diameters in the wake, weakening the wake.</p> <p>Particles are concentrated on the pressure side and mainly on 50% of the blade near the hub.</p> <p>With increased air velocity, particles move closer to the hub and appear on the upper surface, causing erosion.</p>

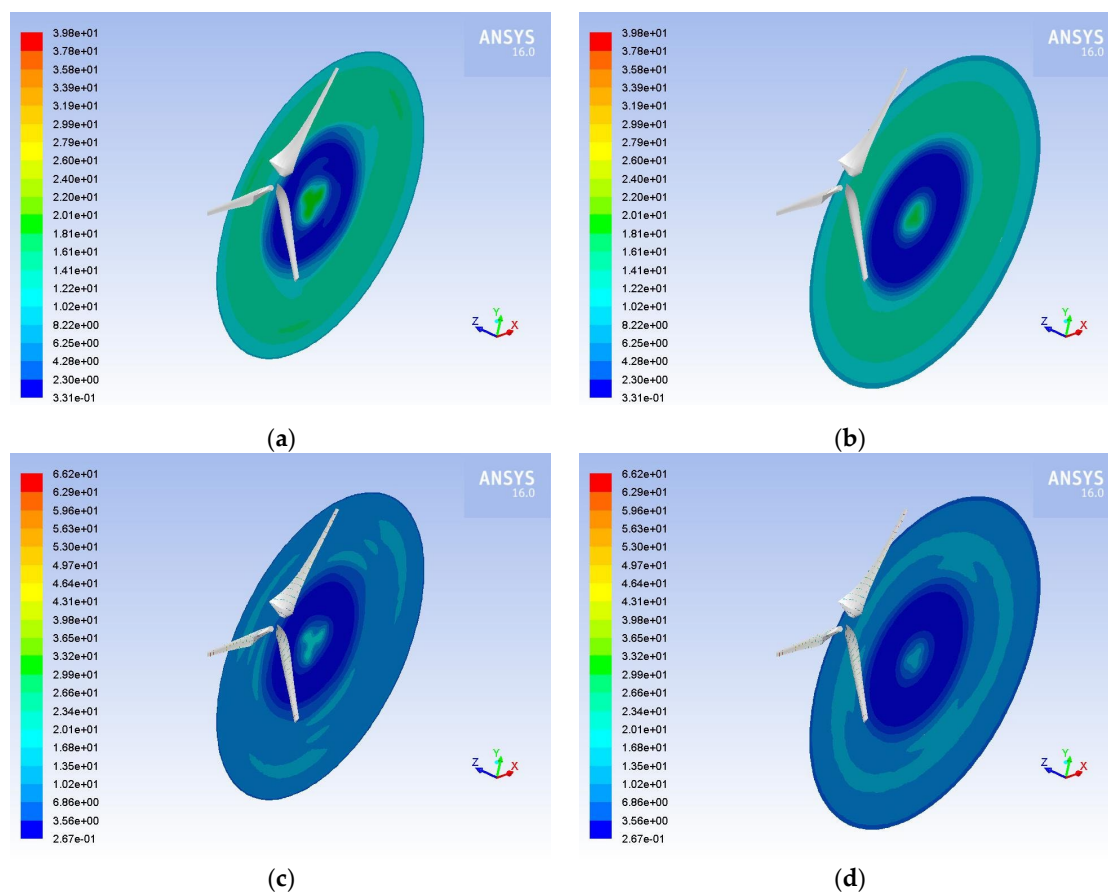


Figure 10. Velocity contours downstream from the three-bladed HAWT rotor at (a) 15 m; (b) 30 m; for airflow and at (c) 15 m; (d) 30 m for hailstorm conditions and wind speed of  $10 \text{ m}\cdot\text{s}^{-1}$  [126].

### 3.4. Dust and Sand

In regions with warm and dry climates, sand and dust often represent prevalent airborne particles, which potentially result in LE erosion concerns (Figure 11). However, in greener and wetter environments, this problem might not exist. Additionally, coastal areas may face significant threats from sand erosion. In general, dust accumulation on the blade surface can increase drag force and reduce lift force, ultimately reducing power output.

The first serious discussions and analyses of blade surface roughness caused by dust accumulation on HAWT performance emerged in 2007 with Khalfallah and Koliub [127]. Their experimental investigation focused on a stall-regulated, 300 kW HAWT, analyzing the mechanism of dust buildup and accumulation on the blade surface over the turbine's operational period. Furthermore, the research evaluated the impact of dust on the performance of a pitch-regulated 100 kW HAWT and compared these findings with those of the 100 kW stall-regulated HAWT. They concluded that the effect of dust on HAWTs depends on various factors, including rotor speed and specifications, nacelle height from the ground, power-regulation type, and wind farm site conditions.

Khakpour et al. [128] examined the way that sand particles impact the performance of the primary airfoil in a HAWT. They compared the flow pattern and pressure distribution in dusty conditions to those in uniform flow, considering different AOAs. The findings demonstrate that introducing sand particles reduces the pressure coefficient on the airfoil, leading to lower drag coefficients. This effect is more pronounced with fine sand particles and diminishes gradually as the particles become coarser. The lift coefficient shows little sensitivity to changes in sand particles, except at high AOAs. At high AOAs, small particles result in the highest erosion rate, while coarse particles cause maximum erosion at zero AOA. Their study also investigated the effects of different sand-to-air drift velocities. The results indicate that larger drift velocities yield more noticeable changes. Furthermore, when examining various sand-to-air mass flow rate ratios, it becomes evident that the discrete phase formulation is inaccurate as it fails to consider the effects of particle collisions. However, the findings regarding pressure distribution demonstrate that increasing particle mass flow rate ultimately decreases the pressure coefficient, particularly in the downstream region.

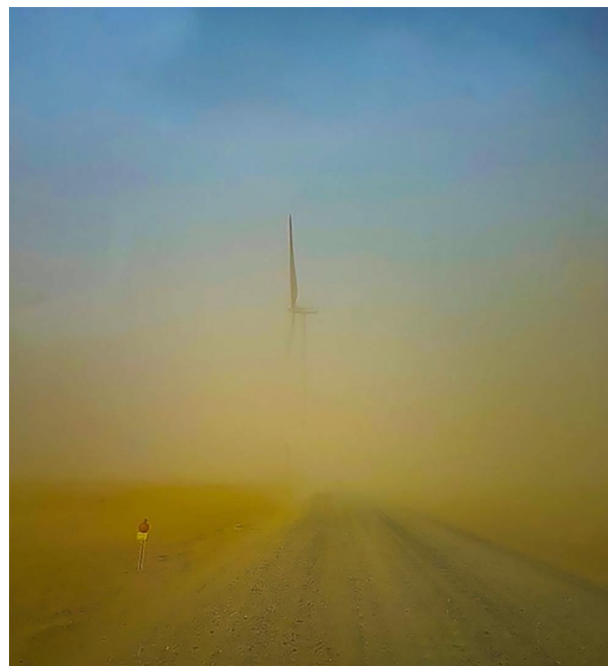


**Figure 11.** View of the Shagaya wind farm from the control building, 150 m away from the nearest turbine, during a severe storm on 26 April 2018. Reproduced with permission from [129], Elsevier, 2018.

Several researchers used the 2D Navier–Stokes equations and the SST  $k$ - $\omega$  turbulence model to simulate the aerodynamic characteristics of a large number of HAWT airfoils operating in a dusty environment. Ren and Ou [130] numerically studied the flow past NACA 63-430 airfoil, a common HAWT airfoil, under both clean and rough surface conditions. Lift and drag coefficients of the NACA 63-430 airfoil were computed for varying roughness heights, locations, and areas, corresponding to the buildup of dust on HAWT blade surfaces during their operation in natural environments and highlighting their role in promoting the transition to turbulence and flow separation. Critical values for roughness height, area, and location were determined. The airfoil's performance under different operational periods was simulated, leading to a recommended cleaning frequency of 3 months without rain for HAWT blade surfaces. The study revealed that airfoil performance is highly affected by small roughness height, and, particularly for the NACA 63-430 airfoil, the location of roughness within the front 50% of the chord length has a significant impact on its performance.

Li et al. [131] studied, also computationally, another airfoil used in HAWT blade construction, the DU 95-W-180 airfoil. Their study examined the impact of surface roughness on airfoil performance, including lift and drag coefficients under various roughness heights, ranging from 0.03 mm to 2 mm, and locations. Critical values for roughness height and location were identified, with critical roughness equal to 0.5 mm. On the suction surface, the critical locations are situated at 10% of the chord length, while on the pressure surface, they are located at 100% of the chord length. The study explored how lift and drag coefficients changed according to roughness height at these critical locations. It was found that for a smooth surface of up to 0.5 mm roughness height, the lift coefficient increases and the drag coefficient decreases rapidly. For a roughness height higher than 0.7 mm, the aerodynamic coefficients' change is slower.

Salem et al. [132] developed a CFD model merged with a deposition model to evaluate the performance degradation of HAWTs, with an NACA 63-215 airfoil, operating in the dusty regions of North Africa and the Middle East. Their results agreed well with the results of Ren and Ou [130] and Li et al. [131], and they proposed the same frequency of blade cleaning as Ren and Ou [130]. They concluded that roughness contributes to the premature transition to a turbulent boundary layer.

Wu et al. [133] simulated the impact of the presence of contaminants on the surface of a HAWT airfoil, the FFA-W3-211 airfoil, on their aerodynamic characteristics. The airfoil surface was evenly roughened, with roughness heights ranging from 0.03 mm to 2.0 mm. By dividing the airfoil into 18 sections, the lift and drag coefficients were analyzed, as the locations of significant roughness varied. To determine the airfoil's sensitivity, the results obtained from XFOIL and CFD calculations were compared. Consequently, the areas of the airfoil surface that were most affected by surface roughness were identified, both on the suction site (at 53% and 92% distances from the chord line towards the LE) and the pressure site (at 44% and 88% distances). The presence of sensitive roughness at these locations caused a delay in the transition point.

Fiore and Selig [134,135] conducted a numerical investigation simulating collisions of sand grains on a 1.5 MW HAWT blade, constructed by DU 97-W-300, DU 96-W-212, and DU 96-W-180 airfoils along the blade. The goal of sand simulations is to ascertain the rate of surface erosion. The findings suggest that the locations where particles impact the blade sections depend on the airfoil type, the local AOA, the local freestream velocity, and the particles. Sand particles predominantly collided in the vicinity of the blade's LE and the erosion rate was highest on the low-pressure side of the HAWT blade. The erosion rate at a radial position of  $r/R = 0.75$  exhibited an approximately tenfold increase compared to the inboard section located at  $r/R = 0.35$ . In the vicinity of the LE, steep angles of impact were observed, resulting in a minimum erosion rate. However, as the blade section moved slightly downstream, the erosion rate reached its maximum value.

Fiore and Selig [136] optimized HAWT airfoils, which are subjected to erosion due to the collision of sand grains on the LE of the rotor blades. For the optimization, a genetic

algorithm was coupled with XFOIL and BugFoil. The impact of sand impingement on the blade surface generates two distinct erosion peaks situated at a certain distance from the LE. These erosion peaks are susceptible to displacements influenced by factors such as the AOA, diameter of sand particles, and velocity inlet. The study also examined the impact of different airfoil shapes on erosion rates. The results revealed that a bulbous upper LE facilitates downstream movement of the erosion rate peak, whereas a flat slanted inclined lower surface of the LE allows particles to decelerate, resulting in surface impacts at nearly perpendicular angles.

Fiore and Selig [137] used a time-stepping algorithm to predict the final form of HAWT blades affected by erosion caused by sand and determined the key factors influencing blade lifespan. The most significant factor was the sand particle's diameter, with the lifespan of the blade decreasing parabolically as the particle's diameter increases. The blade's lifespan is influenced positively for higher lift coefficients and turbine hub heights. Furthermore, the longest observed lifespans were found for airfoils with bulbous and rounded LEs, along with moderately aft-cambered airfoils.

Diab et al. [138] compared the contamination sensitivity of various airfoil shapes, DU NACA, and NREL, commonly used in HAWT blades and investigated the potential application of an LE slat in a NACA airfoil to alleviate the HAWT performance deterioration due to dust. The thickness to chord ratios of the studied airfoils were ~15%, ~20%, and ~25%. The flow of particles over the airfoil section was simulated by the help of the SST  $k-\omega$  turbulence model and DPM. The findings suggest that HAWT airfoils designed with low surface contamination sensitivity exhibit superior performance under dusty conditions. Additionally, the introduction of an LE slat impacts the aerodynamics of the particle-laden flow, offering a potential solution to mitigate the detrimental effects of surface contamination, which would otherwise necessitate costly frequent cleaning.

Srinivasan and Surasani [139] examined the way that surface fouling affects NREL S814 and NREL S826 airfoils, at two Reynold's numbers. Surface fouling was simulated by adding roughness at the LE of the airfoil. The research findings indicate that the transition model accurately predicts flow over clean airfoils, while the fully turbulent model provides a more precise representation of surface-fouled conditions. A comparison between normal operating conditions and surface-fouled conditions reveals that the Reynold's number does not significantly impact the aerodynamic characteristics of either airfoil. Furthermore, the S826 airfoil, which is thinner, demonstrates greater resistance to performance degradation caused by surface fouling compared to the S814 airfoil.

Jafari et al. [140] numerically studied the viscous and turbulent flow over an E387 airfoil and a turbine blade. The primary aim of their study was to explore different arrangements of roughness to minimize the negative effects caused by rough surfaces. To achieve this, sand grain roughness was evenly distributed along the suction side, the pressure side, and both sides during manufacturing. Their findings suggest that, contrary to previous research, applying roughness exclusively to the pressure side of the airfoil proves beneficial. Under this configuration, the lift coefficient increases by 8.62% compared to an airfoil with rough surfaces and by 1.2% compared to an airfoil with smooth surfaces. However, the lift coefficient of the blade with roughness on the pressure surface is slightly lower than the smooth blade, but the detrimental effects are considerably less compared to having roughness on the suction surface or on both sides.

Zidane et al. [141] examined the impact of debris flow on the efficiency of HAWT blades. The aerodynamic characteristics of a NACA 63415 airfoil is analyzed using 2D incompressible Navier–Stokes equations and the SST turbulence model, considering both clean and sandy conditions. By utilizing DPM, the study investigates the influence of sand particles on aerodynamic characteristics. Varying flow rates of sand particles are studied to determine their impact on the airfoil's pressure and lift coefficients. The airfoil's performance is evaluated at different AOAs, ranging from  $0^\circ$  up to  $10^\circ$ . Findings demonstrate that the blade's lift coefficient can decrease by 28% during sandstorms comparable to those experienced in the Gulf and South African countries.

Han et al. [142] quantitatively analyzed the impact of contamination and erosion on the AEP of HAWTs. Transient CFD simulations of the NACA 64-618 airfoil provided the relevant aerodynamic data, which were then applied to the tip area of the 5-MW NREL reference HAWT model to calculate the corresponding AEP losses. Blades with contaminant accumulation at the airfoil's LE experienced a decrease of up to 27% in lift coefficient and an increase of up to 159% in drag coefficient compared to a clean airfoil. On the other hand, blades affected by erosion at the LE exhibited a decrease of up to 53% in lift coefficient and an increase of up to 314% in drag coefficient. The reduction in aerodynamic characteristics was more pronounced in the section exposed to large AOAs ( $10^\circ$  and higher), particularly with a greater extent of surface damage at the LE. In general, the computed AEP reduction varied between 2% and 3.7%, based on the degree of damage observed at the LE.

Chen and Agarwal [143] studied, computationally, the aerodynamic characteristics of the S809 and S814 airfoils in clean and dusty air conditions. In the case of clean air, the Spalart–Allmaras and the Realizable  $k-\epsilon$  turbulence models were employed, and the obtained results were compared with experimental data to determine the preferable model. In dusty air conditions, the Realizable  $k-\epsilon$  model and DPM were used, considering two different dust particle concentrations, 1% and 10% per volume. The results were compared with the clean air data to demonstrate the impact of dust contamination on the airfoil's aerodynamic characteristics, and they concluded that the power degradation of HAWTs was more severe for the 10% concentration of particles.

Guo et al. [144] simulated air–particle flows over S809, NH6 MW25, and NACA 0012 airfoils. The results showed that a slight decrease in performance occurs in attached flow due to momentum loss in the boundary layer. However, when flow separation occurs, the performance degradation becomes more severe, primarily due to a more extensive separation caused by particles. In contrast to the NACA 0012 airfoil, the other two airfoils exhibit a specific AOA in the light stall region that is most sensitive to particles. At this angle, the decrease in lift and the increase in drag reach their peak values. For the S809 airfoil, the most sensitive AOA is approximately  $3^\circ$  greater than the maximum lift-to-drag ratio angle. They concluded that the presence of particles has a significant impact on the aerodynamic characteristics of HAWTs.

ElMessiry et al. [145] numerically studied the impact of dust on the aerodynamic characteristics of the same airfoil families with the same thickness to chord ratios as Diab et al. [138]. The results revealed that fouled airfoils generally experienced a decrease in lift coefficient, ranging from 17% to 75%, along with an increase in drag coefficient compared to the clean conditions. Most airfoils demonstrated a 40% drop in lift coefficient. Among airfoils operating in clean conditions, the DU 84-132V3 displayed the greatest performance, although it cannot guarantee the same level of performance when exposed to dusty environments, which can alter the airfoil's geometry. The NACA 63-215 airfoil demonstrated the least sensitivity to dust accumulation, exhibiting excellent performance across different AOAs and only experiencing a minor decrease in aerodynamic characteristics compared to other airfoils.

Douvi et al. numerically investigated the aerodynamic characteristics of the S809 [146,147] and NACA 0012 [148,149] airfoils within a Reynolds number range of  $1 \times 10^6$  to  $3 \times 10^6$  while considering different concentrations of sand particles in the airflow. The findings revealed that irrespective of the airfoil type and Re, an increase in AOA and sand particle concentration leads to elevated degradation of performance. Based on the examination of a three-bladed HAWT with blades utilizing these airfoils, it has been observed that the inclusion of sand particles leads to a reduction in the power coefficient, influenced by both the twist angle of the blades and the concentration of sand particles in the airflow. Moreover, the concentration of sand particles suggested a tendency for particle accumulation predominantly on the upper surface and in the region extending from the LE to the central area of the lower surface, particularly at small angles of attack. As the AOA increases, particle concentration narrows down to a smaller section of the airfoil.

Douvi et al. [150] studied the aerodynamic efficiency of a HAWT operating in a dusty environment with varying dust concentrations in the airflow. An optimized rotor for a three-bladed HAWT, constructed with S809 airfoil blades, was calculated using the user-friendly TTBEEM application [118] and designed by QBlade [151]. Additionally, numerical simulation was carried out, with the MRF model accounting for blade rotation and the DPM model handling dust injection into the flow field. The results of this investigation confirmed that the aerodynamic performance of a HAWT is negatively affected when operating in dusty environments. Depending on the conditions, the power output of the HAWT was found to decrease by between 1.24% and 9.04%. The illustration of the flow field revealed that as the concentration of sand particles in the air increased, the wake became weaker and the minimum velocity values decreased. At higher wind speeds, the velocity distribution pattern remained consistent, but the range of values increased, and the wake dissipated more rapidly. Furthermore, sand particles tended to accumulate more towards the hub, and as the concentration and wind speed increased, the particles on the rotor became more abundant (Figure 12). Moreover, it was observed that the particles were mainly dissipated near the LE along the blade and on the pressure surface, where static pressure reached its highest values. Moving towards the hub, the particles concentrated over a larger area on the blade's pressure surface, negatively impacting the power produced by the HAWT. The regions with the highest dissipation rate of sand coincided with those with the highest erosion rate (Figure 13).

Zare et al. [152] used numerical methods to examine the performance of the NREL Phase VI HAWT, operating under clean and dusty air. They investigated how the aerodynamic performance of the turbine is affected by variables such as wind speed (from 5 to 25 m/s), particle diameter (from 0.025 to 0.9 mm), and AOA (from  $0^\circ$  to  $44^\circ$ ). Their findings reveal that the HAWT's performance declines in dusty conditions, particularly for particle diameters larger than 0.1 mm and when it is in a post-stall state. The power generated decreases on average by 4.3% and 13.3% for air with particles of 0.05 mm and 0.9 mm diameter, respectively. The presence of particles significantly alters the flow field, resulting in a reduced pressure difference between the suction and pressure sides of the blade, an increased separation of the boundary layer, and strengthened recirculation zones. Various airfoil and HAWT types tested under sand conditions are compiled in Table 5.

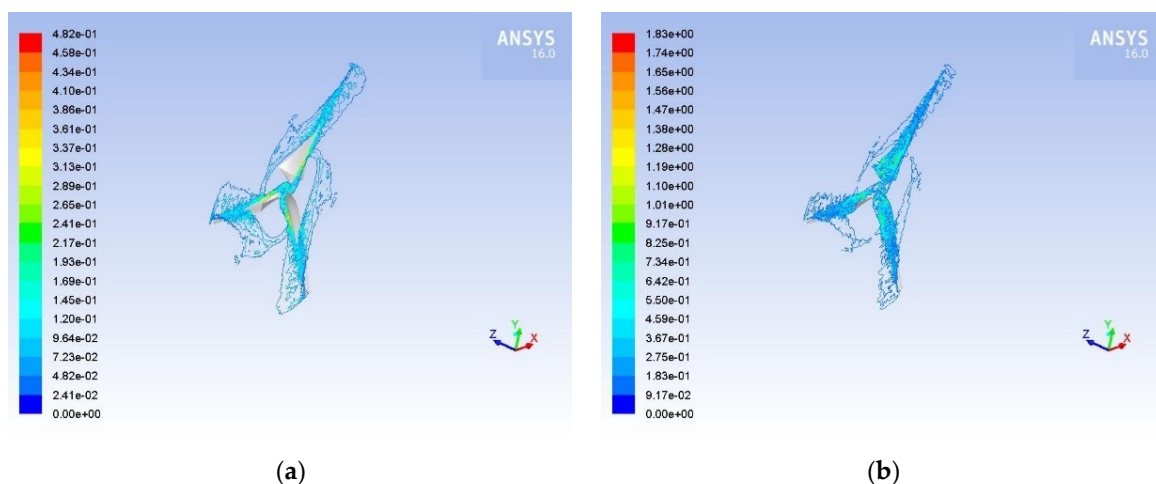


**Figure 12.** Sand particles' concentration close to the three-bladed HAWT rotor at (a) wind speed  $10 \text{ m}\cdot\text{s}^{-1}$  and particle concentration 5%; (b) wind speed  $10 \text{ m}\cdot\text{s}^{-1}$  particle concentration 10% [150].

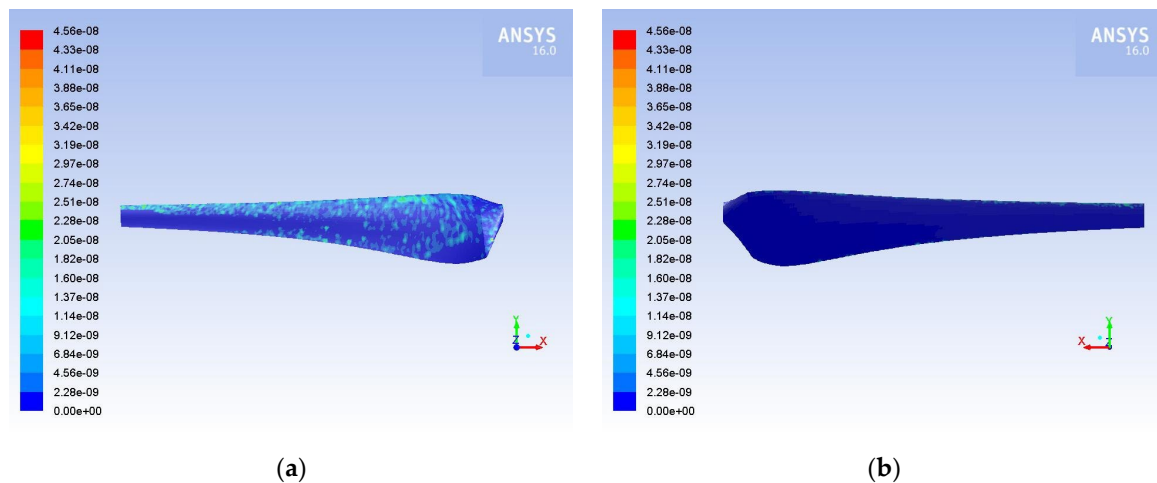


**Figure 13.** Erosion rate of the three-bladed HAWT rotor blade (a) pressure; (b) suction side for wind speed  $15 \text{ m}\cdot\text{s}^{-1}$  particle concentration 10% [150].

**Table 5.** Various airfoil and HAWT types tested in bibliography for sand conditions.

Author	Investigation Method	HAWT or Airfoil Type	Main Conclusions
Khalfallah and Koliub [127]	experimental	Nordtank 300 kW HAWT	The impact of dust on HAWTs depends on rotor speed, specifications, nacelle height, power regulation, and wind farm site conditions.
Khakpour et al. [128]	numerical	S819 airfoil	Introducing sand reduces airfoil pressure, lowering drag.
			Fine sand particles have a stronger effect than coarse particles.
			Lift remains mostly unaffected by sand, except at high AOA's.
Ren and Ou [130]	numerical	NACA 63-430 airfoil	Small particles erode the most at high AOA, while coarse particles erode the most at $0^\circ$ .
			Increasing particle mass flow rate lowers pressure coefficient in the downstream region.
			HAWT blade performance is greatly influenced by small roughness height.
Li et al. [131]	numerical	DU 95-W-180 airfoil	Roughness located in the front 50% of the chord length significantly affects performance.
			The lift coefficient reduces by up to 30%, depending on roughness locations.
			It is recommended to clean the blades every 3 months if there is no rain.
Salem et al. [132]	numerical	NACA 63-215 airfoil	For a smooth surface with roughness heights up to 0.5 mm, the lift coefficient increased, while the drag coefficient decreased significantly.
			For roughness heights greater than 0.7 mm, the changes in aerodynamic coefficients were more gradual.
Wu et al. [133]	numerical	FFA-W3-211 airfoil	Their findings aligned with Ren and Ou [130] and Li et al. [131].
			Roughness leads to an early shift to turbulent boundary layer.
Wu et al. [133]	numerical	FFA-W3-211 airfoil	The rough areas on the airfoil surface were at the suction site (53% and 92% from the chord line towards the LE) and the pressure site (44% and 88% distances).
			These rough areas caused a delay in the transition point.

Table 5. Cont.

Author	Investigation Method	HAWT or Airfoil Type	Main Conclusions
Fiore and Selig [134,135]	numerical	1.5 MW HAWT blade, constructed by DU 97-W-300, DU 96-W-212 and DU 96-W-180 airfoils along the blade	The blade sections where particles hit depend on the type of airfoil, AOA, freestream velocity, and particles themselves.
			Sand particles mostly collide near the blade's front edge, causing the highest erosion rate on the low-pressure side.
			At a radial position of $r/R = 0.75$ , the erosion rate increased tenfold compared to the inboard section at $r/R = 0.35$ .
			Steep impact angles were seen near the front edge, minimizing erosion.
			Moving slightly downstream, the erosion rate reached its maximum.
Fiore and Selig [136]	numerical	DU 96-W-180, DU 96-W-212, and DU 96-W-250 airfoils	The erosion from sand impacts creates two peaks on the blade surface, which can shift due to AOA, particle size, and inlet velocity.
			A rounded upper edge helps the erosion peak move downstream, while a flat inclined lower edge causes particles to slow down, resulting in impacts at nearly perpendicular angles.
Fiore and Selig [137]	numerical	DU 96-W-180, S804, S810, S813, S817, S820, S821, S828, and S832 airfoils	The sand particle diameter affects the blade's lifespan. Larger diameters decrease lifespan.
			Higher lift coefficients and turbine hub heights increase lifespan.
			Airfoils with bulbous and rounded LEs, as well as moderately aft-cambered airfoils, have the longest observed lifespans.
Diab et al. [138]	numerical	various types of airfoils	HAWT airfoils designed to be highly resistant to surface contamination perform better in dusty conditions.
			Adding an LE slat can reduce the negative impact of dust, avoiding frequent cleaning.
Srinivasan and Surasani [139]	numerical	S814 and S826 airfoils	The transition model accurately predicts flow over clean airfoils, while the fully turbulent model represents surface-fouled conditions better.
			The Reynold's number does not significantly affect aerodynamic characteristics for either airfoil when comparing normal and fouled conditions.
			S826 airfoil shows better resistance to performance degradation due to surface fouling than S814 airfoil.
Jafari et al. [140]	numerical	E387 airfoil and a turbine blade	Applying roughness only on the pressure side of the airfoil improves the lift coefficient by 8.62% compared to a rough surface and by 1.2% compared to a smooth surface.
			Roughness on the pressure side has a smaller negative impact on the lift coefficient compared to roughness on the suction side or both sides.
Zidane et al. [141]	numerical	NACA 63-415 airfoil	Lift coefficient can decrease by 28% during sandstorm conditions.
Han et al. [142]	numerical	NACA 64-618 airfoil	Blades with sand on their LE had 27% less lift and 159% more drag.
			Eroded blades at the LE had 53% less lift and 314% more drag.
			The impact was worse at high angles ( $10^\circ$ and above) and the damaged area was wider at the LE.
			Energy production dropped by 2% to 3.7%, depending on the level of damage at the LE.
Chen and Agarwal [143]	numerical	S809 and S814 airfoils	10% dust concentration caused more severe power degradation for HAWTs.

Table 5. Cont.

Author	Investigation Method	HAWT or Airfoil Type	Main Conclusions
Guo et al. [144]	numerical	S809, NH6 MW25 and NACA 0012 airfoils	When flow separation happens, the performance degradation worsens due to more extensive separation caused by particles.
			Unlike the NACA 0012 airfoil, the other two airfoils have a specific AOA in the light stall region that is highly influenced by particles.
			For the S809 airfoil, the most sensitive AOA is about 3° higher than the angle for maximum lift-to-drag ratio.
ElMessiry et al. [145]	numerical	same airfoils with Diab et al. [138]	Most airfoils experienced a significant 40% decrease in lift.
			The DU 84-132V3 airfoil performed well under clean conditions, but its performance was uncertain in dusty environments due to changes in the airfoil's geometry.
			The NACA 63-215 airfoil was the least affected by dust accumulation and maintained good performance at different AOAs with only a minor decrease.
Douvi et al. [146,147]	numerical	S809 airfoil	Increasing the AOA and sand particle concentration degrades the performance of a three-bladed HAWT, regardless of Re. The power coefficient decreases due to sand particles, influenced by blade twist angle and particle concentration in the airflow.
Douvi et al. [148,149]	numerical	NACA 0012 airfoil	Sand particles tend to accumulate on the upper surface and from the LE to the central area of the lower surface, especially at small AOAs.
			With higher AOAs, particle concentration narrows to a smaller section of the airfoil.
			The power output of the HAWT decreases by 1.24% to 9.04% depending on conditions.
Douvi et al. [150]	numerical	Optimized three-bladed HAWT, constructed by S809 airfoil blades	As sand particle concentration in the air increases, the wake becomes weaker and minimum velocity decreases.
			Sand particles tend to gather more at the hub, and as concentration and wind speed rise, the particles on the rotor become more abundant.
			Approaching the hub, particles gather over a larger area on the pressure surface, negatively impacting power production.
			The areas with the highest sand dissipation rate correlate with the highest erosion rate.
Zare et al. [152]	numerical	NREL Phase VI HAWT	The HAWT's performance decreases in dusty conditions, especially when it is in a post-stall state and for particle diameters > 0.1 mm.
			The average power generated decreases by 4.3% and 13.3% for particles with diameters of 0.05 mm and 0.9 mm, respectively.
			Particles significantly change the flow, reducing the pressure difference between the blade's suction and pressure sides, increasing the separation of the boundary layer, and strengthening recirculation zones.

### 3.5. Insects

In high winds, the presence of flying insects around turbines is infrequent, ensuring that HAWTs operating under steady high-wind conditions stay free from contamination, thereby maintaining constant power levels. However, during high winds, the angle formed between the airflow and the blades increases, causing the aerodynamic suction peak to shift towards the LE. If the LE is already covered with deceased insects from a prior low-wind period, the resulting power output will decrease. The level of contamination at the suction peak directly affects blade stall and lift loss. Consequently, after each low-wind period, the amount of insect contamination may vary, leading to different power levels being

produced in high winds [7]. Figure 14 shows a close view of the contamination of insects on a HAWT blade.

In recent times, the impact of insect contamination on HAWT performance has gained recognition, although it was not previously regarded as a significant cause of power loss. Observations at wind farms in California [7,153] revealed varying power levels among different turbines operating under the same wind speed.



**Figure 14.** Contamination of insects on HAWT blade [154].

To investigate this phenomenon, Corten and Veldkamp [153] proposed and experimentally tested multiple hypotheses. Among these, they confirmed the plausibility of insect accretion on HAWT blades, primarily occurring during low-speed winds when insects are capable of flight. At such speeds, the roughness caused by insects has a negligible effect on power production. However, at higher wind speeds, there is a notable decline in power output due to the increased surface roughness resulting from insect contamination. Furthermore, the level of contamination is found to rely on atmospheric conditions during insect flight, particularly when the temperature is above 10 °C and there is no rain. Additionally, insect density decreases rapidly from ground level to an altitude of 150 m [155]. Insect-free environments are more prevalent in very low temperatures and low humidity [156]. The conditions conducive to insect contamination are illustrated in Figure 15. The observed increase in the power curve is attributed to the cleaning effect of rainfall on the turbine blades.

To ascertain the validity of the hypothesis, an experimental investigation was conducted utilizing two adjacent HAWTs situated within the same wind park. The initial HAWT, designated as the clean HAWT, underwent natural exposure to insect contamination, while an artificial surface roughness was intentionally introduced to the second HAWT. Throughout the experiment, the power outputs of both HAWTs were periodically documented. Initially, the first HAWT exhibited greater power output compared to the second one. However, as the contamination level gradually escalated, the power output of the first HAWT progressively declined, eventually aligning with the power production of the second one, which means that the accumulation of natural contamination resulted in a degree of surface roughness equivalent to that of the second HAWT. These findings effectively confirm the hypothesis that the accumulation of insects on the blade surface, by augmenting its roughness, results in a reduction in power output [153].

Janiszewska et al. [157,158] experimentally studied the LS(1)-0417MOD and S814 airfoils under clean and rough conditions. Field measurements on the LE area of a HAWT blade uncovered that the average grain size of the typical roughness resulting from insect contamination on HAWT blades ranged from 0.5 mm to 0.9 mm. The density of these rough elements varied from 1.25 to 5 particles per cm<sup>2</sup>. The roughness design was based on the measurements from the HAWT, leading to a 41% and 24% decline in maximum

lift coefficient and a 36% and 60% increase in minimum drag coefficient, for the LS(1)-0417MOD airfoil and the S814 airfoil, respectively. Similar wind tunnel experiments were performed on the NACA 4415, S801, S809, and S813 airfoils [159–162] using the same roughness design as Janiszewska et al. [158]. The results indicated reductions of up to 20%, 12%, 19%, and 12% in the maximum lift coefficient for the NACA 4415, S801, S809, and S813 airfoils, respectively, and an increase greater than 50% for all airfoils tested.

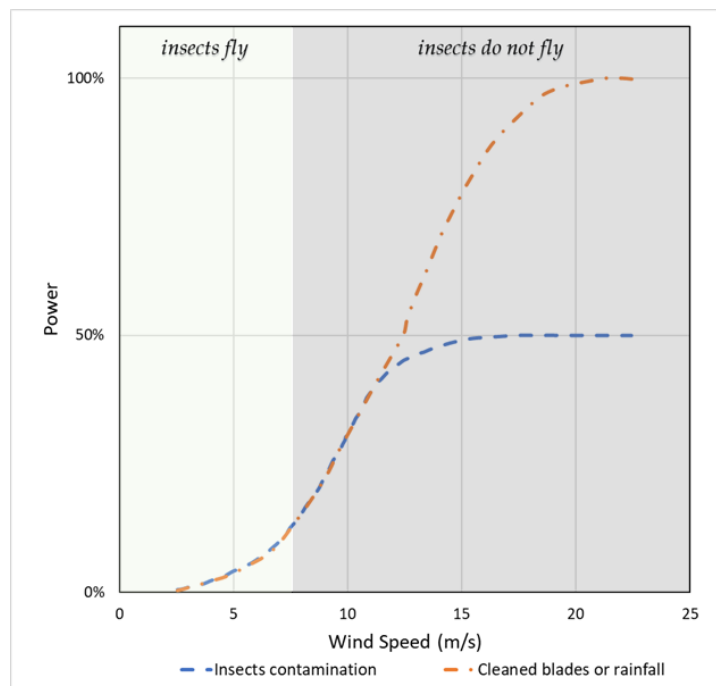


**Figure 15.** Conditions promoting insect contamination.

Ferrer and Munduate [163] conducted CFD analyses to determine S814 airfoil performance under clean and rough surfaces, by simulating contamination during the operational lifespan of HAWTs. The roughness pattern for the S814 tests was a molded insect pattern sourced from an actual HAWT in the field and the results agreed with the corresponding data from Janiszewska et al. [158]. The results indicate that contamination-induced roughness has a more detrimental impact on the aerodynamic behavior of the airfoil than boundary layer transition. The aerodynamic degradation reached 60% for the lift-to-drag ratio for moderate AOAs.

Wilcox et al. [164] developed a simulation code to establish the connection between airfoil type, insect collision areas, and roughness sensitivity. They determined representative insect collection patterns for various airfoil shapes and used these data to simulate roughness on an NREL S814 airfoil, which was tested, experimentally, at various Reynolds numbers. The obtained results were compared to the results of Ehrmann [165] for the NACA 63<sub>3</sub>-418 airfoil. The analysis revealed that increasing roughness density and height led to a reduction in the maximum lift, lift-to-drag ratio, and lift curve slope. It was pointed out that the S814 airfoil exhibited heightened sensitivity to roughness in comparison to the NACA 63<sub>3</sub>-418 airfoil. To quantify the AEP losses, blade element momentum analysis was employed. It was determined that an NACA 63<sub>3</sub>-418 HAWT experienced a 4.9% decrease in energy production, while an S814 HAWT encountered a slightly higher reduction of 6.8%.

Fiore and Selig [134,135] numerically studied, in addition to the sand grains, the collisions of insects on a 1.5 MW HAWT blade. The debris thickness on the blade was estimated through insect simulations. The findings suggest that the locations of particle impact on the blade sections are influenced by factors such as the airfoil type, the local AOA, the local freestream velocity, and the particles. Collisions between insects and sand

grains were predominantly observed near the LE of the blade. The highest volume of insect debris per unit span was found at  $r/R = 0.75$ .

### 3.6. Other Aspects

#### 3.6.1. Humidity

In recent years, there has been a rise in the installation of large offshore HAWTs to harness the considerable potential of wind energy. Although offshore wind resources are plentiful, stronger, and more consistent compared to those on land, offshore HAWTs typically operate in environments with high humidity. Consequently, the measurement of the HAWT power curve based on the IEC standard is conducted onshore, often in environments with lower to moderate humidity.

When the air contains a significant amount of moisture, it can lead to condensation on the surface of the rotating blades. This condensation, especially during winter weather, can result in reduced blade performance due to contamination or the formation of ice. Additionally, in the mornings, foggy or rainy conditions are frequent around offshore wind farms. These conditions cause tiny water droplets to mix with the air, and when they collide with the rotating blades, it increases drag and negatively affects turbine performance. Offshore HAWTs are more prone to corrosion due to exposure to seawater and high humidity. Consequently, they need to be designed with greater durability to minimize maintenance, mainly because the transportation of maintenance crews and replacement parts to and from offshore wind plant sites incurs high costs.

Yu et al. [166,167] simulated the effects of different humidity levels on airfoil/blade aerodynamics and the impact of water condensation on HAWT blades. Their analysis revealed that high humidity significantly affects density under high-temperature conditions but has minimal impact on airfoil/blade aerodynamics. Additionally, water vapor condensation occurs on the airfoil or blade surfaces, primarily around the LE and TEs. This phenomenon leads to blade contamination, particularly in dirty environments with dust and insects, or during winter and low-temperature conditions conducive to icing. When contamination occurs, the performance of the HAWT can be considerably degraded. Their study also found that on foggy days, water droplets in humid air contaminate on the airfoil surface, forming a water film that alters the flow of the boundary layer, leading to increased drag and diminished performance. The findings from these studies are confirmed by similar findings of performance losses on rainy days.

#### 3.6.2. Sea Spray

The impact of sea spray on offshore HAWTs is a significant concern, specifically regarding the LE of the HAWT blades. The effects of sea spray on the blades are expected to resemble those of rain, involving forces, pressures, and discrete impact events. In certain cases, the blades can be quickly affected by larger amounts of seawater spray. Another aspect to consider when dealing with the impact of particles is the existence of sea salt crystals within the spray. Airborne sea salt crystals pose a challenge in various offshore applications, primarily leading to their accumulation on components. The problem of salt-contaminated blades was considered during the study of lightning protection measures for HAWTs [168–170]. Moreover, since seawater typically contains 3–3.5% NaCl [171], corrosion becomes a significant concern for metallic elements. Consequently, the accumulation of salt crystals on the LE of the blade results in deterioration in aerodynamic characteristics and potentially in corrosive damage. Despite its significance, limited research has been conducted on this subject thus far.

## 4. Conclusions

The escalating effects of global climate change, including the rise in greenhouse gas concentrations and the depletion of fossil fuel reservoirs, have spurred a substantial surge in the demand for alternative energy sources. Among these, wind energy stands out as a highly promising solution due to its comparatively lower cost and minimal environmental

impact. It is crucial to examine the impact of various meteorological phenomena on the performance of typical HAWTs as this knowledge is essential for enhancing their design and overall efficiency.

The aim of the present research was to examine the changes in the aerodynamic characteristics of HAWTs operating under hazard environmental conditions. Various conditions were reviewed, such as icing, rainfall, hailstorms, high concentrations of dust, humidity, insect collisions, and sea spray.

All of the studies reviewed here support the hypothesis that when HAWTs operate under these conditions, they experience a decrease in lift and a simultaneous increase in drag, which leads to aerodynamic characteristics' degradation. Since the aerodynamic performance is directly connected to the power output of HAWTs, efforts should be implemented to mitigate these losses.

Researchers have dedicated significant attention to the study of ice accumulation and its impact on the aerodynamic characteristics of airfoils and blades. The research on this topic is popular in cold regions, such as Norway and Canada. More extensive research has been conducted involving ice due to the convenient observation of ice formation on blades in such locations, allowing for experimental study of its effects. Consequently, computational simulation of ice conditions was relatively uncomplicated, as the study involved altering the geometry while assuming the presence of formed ice.

Conversely to ice, there is a scarcity of experimental research in the literature concerning the performance of HAWTs in rainy conditions. When HAWTs are subjected to rainy conditions, rain droplets accumulate on the surfaces of the blades or airfoils, subsequently causing a decline in aerodynamic performance.

To perform a thorough examination of HAWT performance under various operating and environmental conditions, the DPM, which is available in CFD codes, is highly suitable for delivering accurate and intricate insights into turbine performance. This method obviates the need for expensive experimental setups at different scales by offering comprehensive and reliable information. The data obtained through the CFD approach can be utilized to optimize HAWT design, operations, and scale-up processes. This model has been used extensively to simulate the rainfall, the hailstorms, and the dust over a HAWT blade. The degradation of the aerodynamic characteristics of a HAWT is more pronounced when faced with heavier and larger raindrops, hailstones, and sand particles, as well as a higher LWC and sand concentration in the air. However, a comprehensive understanding of the aerodynamic characteristics of offshore HAWTs in high humidity environments and in regions with sea salt remains lacking.

Countries with the most operational wind farms exhibit a notable inclination towards HAWT operation under hazard conditions, as evident from the map in Figure 16. Moreover, several airfoil types were studied, and the most popular was the S809 airfoil followed by NACA 0012 and NACA 64-618 (Figure 17).

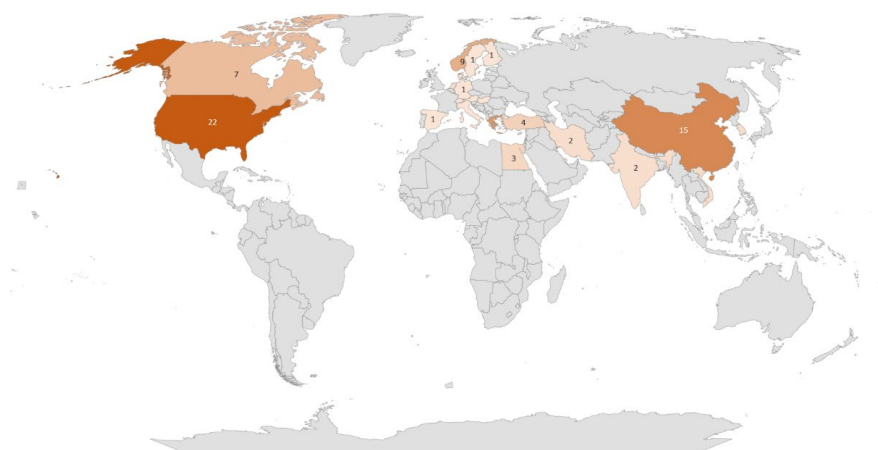


**Figure 16.** Institutions globally that have studied the operation of HAWTs under hazard conditions.

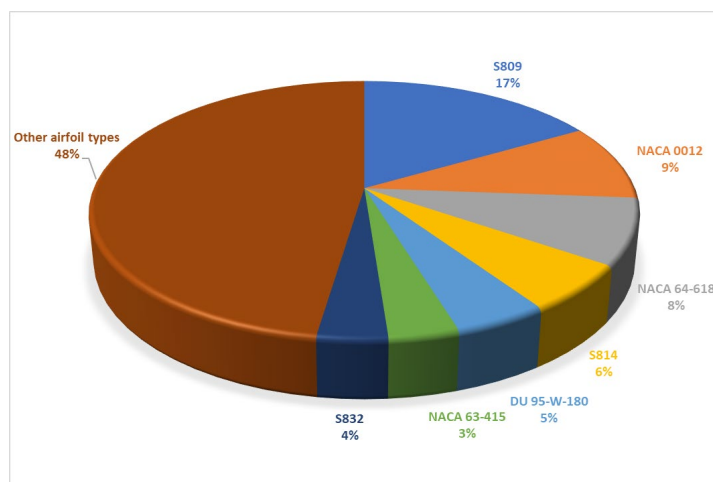


**Figure 17.** Airfoils used for the construction of HAWT blades investigated operating under hazard conditions.

In the field of the operation of HAWTs under hazardous conditions, several unresolved issues remain and need further investigation in the near future. Some of these include:

- The operation of HAWTs in various hailstorm conditions and in environments with sea spray;
- The design and analysis of additional airfoils and HAWT blades, aiming to optimize their performance across hazard environmental conditions;
- Employing user-defined functions (UDFs) to introduce particles of varying shape and size, facilitating the study of multiphase flows;
- Investigating the impact of these multiphase flows in wind farms, specifically in conjunction with terrain; this case would necessitate significant computational power.

**Funding:** This research received no external funding.

**Data Availability Statement:** Not applicable.

**Conflicts of Interest:** The authors declare no conflict of interest.

## References

1. Intergovernmental Panel on Climate Change (IPCC). *Renewable Energy Sources and Climate Change Mitigation*; Cambridge University Press: Cambridge, UK, 2011.
2. IRENA. *Renewable Capacity Statistics 2023*; International Renewable Energy Agency: Abu Dhabi, United Arab Emirates, 2023.
3. IEA. *Renewable Energy Market Update—June 2023*; IEA: Paris, France, 2023.
4. Global Energy Monitor. *Global Wind Power Tracker*; Global Energy Monitor: Covina, CA, USA, 2023.
5. Papiez, M.; Smiech, S.; Frodyma, K. Factors affecting the efficiency of wind power in the European Union countries. *Energy Policy* **2019**, *132*, 965–977. [[CrossRef](#)]
6. Dalili, N.; Edrissy, A.; Carriveau, R. A review of surface engineering issues critical to wind turbine performance. *Renew. Sustain. Energy Rev.* **2007**, *13*, 428–438. [[CrossRef](#)]
7. Corten, G.V.H. Insects can halve wind-turbine power. *Nature* **2001**, *412*, 41–42. [[CrossRef](#)]
8. Moroz, E.; Eggleston, D. A comparison between actual insect contamination and its simulation. *Wind Power* **1992**, *7*, 418–425.
9. Kumar, K.; Safiulla, M.; Ahmed, A. An experimental evaluation of fiber-reinforced polypropylene thermoplastics for aerospace applications. *J. Mech. Eng.* **2014**, *43*, 92–97. [[CrossRef](#)]
10. Amirzadeh, B.; Louhghalam, A.; Raessi, M.; Tootkaboni, M. A computational framework for the analysis of rain-induced erosion in wind turbine blades, part I: Stochastic rain texture model and drop impact simulations. *J. Wind Eng. Ind. Aerodyn.* **2017**, *163*, 33–43. [[CrossRef](#)]
11. Wu, Z.; Cao, Y.; Nie, S.; Yang, Y. Effects of rain on vertical axis wind turbine performance. *J. Wind Eng. Ind. Aerodyn.* **2017**, *170*, 128–140. [[CrossRef](#)]
12. Castorrini, A.; Corsini, A.; Rispoli, F.; Venturini, P.; Takizawa, K.; Tezduyar, T.E. Computational analysis of wind-turbine blade rain erosion. *Comput. Fluids* **2016**, *141*, 175–183. [[CrossRef](#)]

13. Verma, A.S.; Castro, S.G.; Jiang, Z.; Teuwen, J.J. Numerical investigation of rain droplet impact on offshore wind turbine blades under different rainfall conditions: A parametric study. *Compos. Struct.* **2020**, *241*, 112096. [CrossRef]
14. Mishnaevsky, L.; Hasager, C.B.; Bak, C.; Tilg, A.-M.; Bech, J.I.; Rad, S.D.; Fæster, S. Leading edge erosion of wind turbine blades: Understanding, prevention, and protection. *Renew. Energy* **2021**, *169*, 953–969. [CrossRef]
15. Pryor, S.; Barthelmie, R.; Cadence, J.; Dellwik, E.; Hasager, C.; Kral, S.; Reuder, J.; Rodgers, M.; Veraart, M. Atmospheric Drivers of Wind Turbine Blade Leading Edge Erosion: Review and Recommendations for Future Research. *Energies* **2022**, *15*, 8553. [CrossRef]
16. Pugh, K.; Nash, J.; Reaburn, G.; Stack, M. On analytical tools for assessing the raindrop erosion of wind turbine blades. *Renew. Sustain. Energy Rev.* **2021**, *137*, 110611. [CrossRef]
17. Sareen, A.; Sapre, C.; Selig, M. Effects of leading edge erosion on wind turbine blade performance. *Wind Energy* **2014**, *17*, 1531–1542. [CrossRef]
18. Barfknecht, N.; Kreuseler, M.; de Tavernier, D.; von Terzi, D. Performance analysis of wind turbines with leading-edge erosion and erosion-safe mode operation. *J. Phys. Conf. Ser.* **2022**, *2265*, 032009. [CrossRef]
19. Papi, F.; Cappugi, L.; Salvadori, S.; Carnevale, M.; Bianchini, A. Uncertainty Quantification of the Effects of Blade Damage on the Actual Energy Production of Modern Wind Turbines. *Energies* **2020**, *13*, 3785. [CrossRef]
20. Schramm, M.; Rahimi, H.; Stoevesandt, B.; Tangager, K. The Influence of Eroded Blades on Wind Turbine Performance Using Numerical Simulations. *Energies* **2017**, *10*, 1420. [CrossRef]
21. Manwell, J.; McGowan, J.; Rogers, A. *Wind Energy Explained: Theory, Design and Application*; John Wiley & Sons: Chichester, UK, 2009. [CrossRef]
22. Sagol, E.; Reggio, M.; Ilinca, A. Issues concerning roughness on wind turbine blades. *Renew. Sustain. Energy Rev.* **2013**, *23*, 514–525. [CrossRef]
23. Zidane, I.; Saqr, K.; Swadener, G.; Ma, X.; Shehadeh, M. On the role of surface roughness in the aerodynamic performance and energy conversion of horizontal wind turbine blades: A review. *Int. J. Energy Res.* **2016**, *40*, 2054–2077. [CrossRef]
24. Betz, A. *Introduction to the Theory of Flow Machines*; Pergamon Press: Oxford, UK, 1966.
25. Burton, T.; Sharpe, D.; Jenkins, N.; Bossanyi, E. *Wind Energy Handbook*, 2nd ed.; John Wiley & Sons: Chichester, UK, 2011; pp. 1–780. [CrossRef]
26. Wilson, R.; Lissaman, P.; Walker, S. *Aerodynamic Performance of Wind Turbines*; Oregon State University: Corvallis, OR, USA, 1976. [CrossRef]
27. Parent, O.; Ilinca, A. Anti-icing and de-icing techniques for wind turbines: Critical review. *Cold Reg. Sci. Technol.* **2011**, *65*, 88–96. [CrossRef]
28. Fortin, G.; Perron, J.; Ilinca, A. A study of icing events at Murdochville: Conclusions for the wind power industry. In Proceedings of the International Symposium “Wind Energy in Remote Regions”, Magdalen’s Island, QC, Canada, 19–21 October 2005.
29. EOC Geoservice. GSP—Global SnowPack Mean. Earth Observation Center. Available online: <https://geoservice.dlr.de/web/maps/eoc:gsp:mean> (accessed on 25 May 2023).
30. Turkia, V.; Huttunen, S.; Wallenius, T. *Method for Estimating Wind Turbine Production Losses Due to Icing*; VTT Technology No. 114; VTT Technical Research Centre of Finland: Espoo, Finland, 2013.
31. Ruff, G.; Berkowitz, B. *Users Manual for the NASA Lewis Ice Accretion Prediction Code (LEWICE) (No. NAS 1.26: 185129)*; Lewis Research Center Group: Brook Park, OH, USA, 1990.
32. Marjaniemi, M.; Makkonen, L.; Laakso, T. Turbine-icing model. In Proceedings of the International Conference BOREAS V: Wind Power Production in Cold Climates, Finnish Meteorological Institute, Levi, Finland, 29 November–1 December 2000.
33. Makkonen, L.; Laakso, T.; Marjaniemi, M.; Finstad, K. Modelling and Prevention of Ice Accretion on Wind Turbines. *Wind Eng.* **2001**, *25*, 3–21. [CrossRef]
34. Habashi, W.; Morency, F.; Beaugendre, H. FENSAP-ICE: A comprehensive 3D Simulation Tool for In-flight Icing. In Proceedings of the 7th International Congress of Fluid Dynamics and Propulsion, Sharm-El-Sheikh, Egypt, 19–21 December 2001. [CrossRef]
35. Beaugendre, H.; Morency, F.; Habashi, W. FENSAP-ICE’s three-dimensional in-flight ice accretion module: ICE3D. *J. Aircr.* **2003**, *40*, 239–247. [CrossRef]
36. Wang, Z.; Zhu, C. Numerical simulation for in-cloud icing of three-dimensional wind turbine blades. *Simulation* **2017**, *94*, 31–41. [CrossRef]
37. Jin, J.; Virk, M.; Hu, Q.; Jiang, X. Study of Ice Accretion on Horizontal Axis Wind Turbine Blade Using 2D and 3D Numerical Approach. *IEEE Access* **2020**, *8*, 166236–166245. [CrossRef]
38. Son, C.; Kim, T. Development of an icing simulation code for rotating wind turbines. *J. Wind Eng. Ind. Aerodyn.* **2020**, *203*, 104239. [CrossRef]
39. Li, Y.; Tagawa, K.; Feng, F.; Li, Q.; He, Q. A wind tunnel experimental study of icing on wind turbine blade airfoil. *Energy Convers. Manag.* **2014**, *85*, 591–595. [CrossRef]
40. Jolin, N.; Bolduc, D.; Swytink-Binnema, N.; Rosso, G.; Godreau, C. Wind turbine blade ice accretion: A correlation with nacelle ice accretion. *Cold Reg. Sci. Technol.* **2019**, *157*, 235–241. [CrossRef]
41. Madi, E.; Pope, K.; Huang, W.; Iqbal, T. A review of integrating ice detection and mitigation for wind turbine blades. *Renew. Sustain. Energy Rev.* **2019**, *103*, 269–281. [CrossRef]

42. Pinar Pérez, J.; García Márquez, F.; Ruiz, H. Economic viability analysis for icing blades detection in wind turbines. *J. Clean. Prod.* **2016**, *135*, 1150–1160. [[CrossRef](#)]
43. Ibrahim, G.; Pope, K.; Muzychka, Y. Effects of blade design on ice accretion for horizontal axis wind turbines. *J. Wind Eng. Ind. Aerodyn.* **2018**, *173*, 39–52. [[CrossRef](#)]
44. Martini, F.; Contreras Montoya, L.; Ilinca, A. Review of Wind Turbine Icing Modelling Approaches. *Energies* **2021**, *14*, 5207. [[CrossRef](#)]
45. Bose, N. Icing on a small horizontal-axis wind turbine—Part 1: Glaze ice profiles. *J. Wind Eng. Ind. Aerodyn.* **1992**, *45*, 75–85. [[CrossRef](#)]
46. Rong, J.; Bose, N.; Brothers, C.; Lodge, M. Icing Test on a Horizontal Axis Wind Turbine. *Wind Eng.* **1991**, *15*, 109–113.
47. Han, Y.; Palacios, J.; Schmitz, S. Scaled ice accretion experiments on a rotating wind turbine blade. *J. Wind Eng. Ind. Aerodyn.* **2012**, *109*, 55–67. [[CrossRef](#)]
48. Hu, L.; Zhu, X.; Chen, J.; Shen, X.; Du, Z. Numerical simulation of rime ice on NREL Phase VI blade. *J. Wind Eng. Ind. Aerodyn.* **2018**, *178*, 57–68. [[CrossRef](#)]
49. Gao, L.; Liu, Y.; Hu, H. An experimental investigation of dynamic ice accretion process on a wind turbine airfoil model considering various icing conditions. *Int. J. Heat Mass Transf.* **2019**, *133*, 930–939. [[CrossRef](#)]
50. Gao, L.; Tao, T.; Liu, Y.; Hu, H. A field study of ice accretion and its effects on the power production of utility-scale wind turbines. *Renew. Energy* **2021**, *167*, 917–928. [[CrossRef](#)]
51. Gao, L.; Hu, H. Wind turbine icing characteristics and icing-induced power losses to utility-scale wind turbines. *Proc. Natl. Acad. Sci. USA* **2021**, *118*, e2111461118. [[CrossRef](#)]
52. Li, X.; Jia, Y.; Zhang, H.; Cheng, B. Research on the Change of Airfoil Geometric Parameters of Horizontal Axis Wind Turbine Blades Caused by Atmospheric Icing. *Energy Eng.* **2022**, *119*, 2549–2567. [[CrossRef](#)]
53. Seifert, H.; Richert, F. Aerodynamics of iced airfoils and their influence on loads and power production. In Proceedings of the EWEC'97, European Wind Energy Conference, Dublin, Ireland, 6 October 1997.
54. Jasinski, W.; Noe, S.; Selig, M.; Bragg, M. Wind Turbine Performance Under Icing Conditions. *J. Sol. Energy Eng.* **1998**, *120*, 60–65. [[CrossRef](#)]
55. Hochart, C.; Fortin, G.; Perron, J.; Ilinca, A. Wind turbine performance under icing conditions. *Wind Energy* **2008**, *11*, 319–333. [[CrossRef](#)]
56. Zhao, M.; Jiang, D.; Li, S. Research on fault mechanism of icing of wind turbine blades. In Proceedings of the 2009 World Non-Grid-Connected Wind Power and Energy Conference, Nanjing, China, 24–26 September 2009. [[CrossRef](#)]
57. Homola, M.C.; Virk, M.S.; Wallenius, T.; Nicklasson, P.J.; Sundsbø, P.A. Effect of atmospheric temperature and droplet size variation on ice accretion of wind turbine blades. *J. Wind Eng. Ind. Aerodyn.* **2010**, *98*, 724–729. [[CrossRef](#)]
58. Villalpando, F.; Reggio, M.; Ilinca, A. Numerical Study of Flow Around Iced Wind Turbine Airfoil. *Eng. Appl. Comput. Fluid Mech.* **2012**, *6*, 39–45. [[CrossRef](#)]
59. Hudecz, A.; Koss, H.; Hansen, M. Ice Accretion on Wind Turbine Blades. In Proceedings of the 15th International Workshop on Atmospheric Icing of Structures (IWAIS XV), St. John's, NL, Canada, 8–13 September 2013.
60. Hu, L.; Zhu, X.; Hu, C.; Chen, J.; Du, Z. Wind turbines ice distribution and load response under icing conditions. *Renew. Energy* **2017**, *113*, 608–619. [[CrossRef](#)]
61. Virk, M.; Homola, M.; Nicklasson, P. Effect of Rime Ice Accretion on Aerodynamic Characteristics of Wind Turbine Blade Profiles. *Wind Eng.* **2010**, *34*, 207–218. [[CrossRef](#)]
62. Han, W.; Kim, J.; Kim, B. Study on correlation between wind turbine performance and ice accretion along a blade tip airfoil using CFD. *J. Renew. Sustain. Energy* **2018**, *10*, 023306. [[CrossRef](#)]
63. Jin, J.Y.; Virk, M.S. Study of ice accretion along symmetric and asymmetric airfoils. *J. Wind Eng. Ind. Aerodyn.* **2018**, *179*, 240–249. [[CrossRef](#)]
64. Jin, J.Y.; Virk, M.S. Study of ice accretion and icing effects on aerodynamic characteristics of DU96 wind turbine blade profile. *Cold Reg. Sci. Technol.* **2019**, *160*, 119–127. [[CrossRef](#)]
65. Jin, J.Y.; Virk, M.S. Experimental study of ice accretion on S826 & S832 wind turbine blade profiles. *Cold Reg. Sci. Technol.* **2020**, *169*, 102913. [[CrossRef](#)]
66. Yirtici, O.; Tuncer, I.H.; Ozgen, S. Ice Accretion Prediction on Wind Turbines and Consequent Power Losses. *J. Phys. Conf. Ser.* **2016**, *753*, 022022. [[CrossRef](#)]
67. Yirtici, O.; Ozgen, S.; Tuncer, I. Predictions of ice formations on wind turbine blades and power production losses due to icing. *Wind Energy* **2019**, *22*, 945–958. [[CrossRef](#)]
68. Yirtici, O.; Cengiz, K.; Ozgen, S.; Tuncer, I.H. Aerodynamic validation studies on the performance analysis of iced wind turbine blades. *Comput. Fluids* **2019**, *192*, 104271. [[CrossRef](#)]
69. Gao, L.; Liu, Y.; Zhou, W.; Hu, H. An experimental study on the aerodynamic performance degradation of a wind turbine blade model induced by ice accretion process. *Renew. Energy* **2019**, *133*, 663–675. [[CrossRef](#)]
70. Jiang, F.; Qiu, T. Research on the effect of icing on aerodynamic performance of airfoil and power generation performance of wind turbine. *J. Phys. Conf. Ser.* **2020**, *1684*, 012141. [[CrossRef](#)]
71. Martini, F.; Ibrahim, H.; Contreras Montoya, L.; Rizk, P.; Ilinca, A. Turbulence Modeling of Iced Wind Turbine Airfoils. *Energies* **2022**, *15*, 8325. [[CrossRef](#)]

72. Chitransh, A.; Kaur, S. Investigation of Single Shot Ice Accretion on Aerofoil of Wind Turbine Blade using ANSYS. In Proceedings of the 2022 International Conference on Smart Generation Computing, Communication and Networking (SMART GENCON), Bangalore, India, 23–25 December 2022. [CrossRef]
73. Rotich, I.; Kollár, L. Numerical simulation of the performance of an asymmetrical airfoil under extreme weather conditions. *Mérnöki Inform. Megoldások* **2022**, *3*, 19–29. [CrossRef]
74. Yang, X.; Bai, X.; Cao, H. Influence analysis of rime icing on aerodynamic performance and output power of offshore floating wind turbine. *Ocean Eng.* **2022**, *258*, 111725. [CrossRef]
75. Virk, M.S.; Nicklasson, P.J.; Homola, M.C. Atmospheric icing on large wind turbine blades. *J. Energy Environ. Eng.* **2012**, *3*, 1–8.
76. Barber, S.; Wang, Y.; Jafari, S.; Chokani, N.; Abhari, R. The Impact of Ice Formation on Wind Turbine Performance and Aerodynamics. *ASME. J. Sol. Energy Eng.* **2011**, *133*, 011007. [CrossRef]
77. Homola, M.C.; Virk, M.S.; Nicklasson, P.J.; Sundsbø, P.A. Modelling of ice induced power losses and comparison with observations. In Proceedings of the Winterwind 2011, Umea, Sweden, 8–10 February 2011.
78. Homola, M.; Virk, M.; Nicklasson, P.; Sundsbø, P. Performance losses due to ice accretion for a 5 MW wind turbine. *Wind Energy* **2012**, *15*, 379–389. [CrossRef]
79. Dimitrova, M.; Ibrahim, H.; Fortin, G.; Ilinca, A.; Perron, J. Software tool to predict the Wind Energy production losses due to icing. In Proceedings of the 2011 IEEE Electrical Power and Energy Conference, Winnipeg, MB, Canada, 3–5 October 2011. [CrossRef]
80. Lamraoui, F.; Fortin, G.; Benoit, R.; Perron, J.; Masson, C. Atmospheric icing impact on wind turbine production. *Cold Reg. Sci. Technol.* **2014**, *100*, 36–49. [CrossRef]
81. Etemaddar, M.; Hansen, M.; Moan, T. Wind turbine aerodynamic response under atmospheric icing conditions. *Wind Energy* **2014**, *17*, 241–265. [CrossRef]
82. Myong, R. Atmospheric Icing Effects on Aerodynamics of Wind Turbine Blade. In Proceedings of the IMECE2013 ASME International Mechanical Engineering Congress and Exposition, San Diego, CA, USA, 15–21 November 2013. [CrossRef]
83. Reid, T.; Baruzzi, G.; Ozcer, I.; Switchenko, D.; Habashi, W. FENSAP-ICE Simulation of Icing on Wind Turbine Blades, Part 1: Performance Degradation. In Proceedings of the 51st AIAA Aerospace Sciences Meeting Including the New Horizons Forum and Aerospace Exposition, Grapevine, Dallas/Ft. Worth Region, TX, USA, 7–10 January 2013. [CrossRef]
84. Shu, L.; Liang, J.; Hu, Q.; Jiang, X.; Ren, X.; Qiu, G. Study on small wind turbine icing and its performance. *Cold Reg. Sci. Technol.* **2017**, *134*, 11–19. [CrossRef]
85. Shu, L.; Li, H.; Hu, Q.; Jiang, X.; Qiu, G.; McClure, G.; Yang, H. Study of ice accretion feature and power characteristics of wind turbines at natural icing environment. *Cold Reg. Sci. Technol.* **2018**, *147*, 45–54. [CrossRef]
86. Shu, L.; Li, H.; Hu, Q.; Jiang, X.; Qiu, G.; He, G.; Liu, Y. 3D numerical simulation of aerodynamic performance of iced contaminated wind turbine rotors. *Cold Reg. Sci. Technol.* **2018**, *148*, 50–62. [CrossRef]
87. Zanon, A.; De Gennaro, M.; Kühnelt, H. Wind energy harnessing of the NREL 5 MW reference wind turbine in icing conditions under different operational strategies. *Renew. Energy* **2018**, *115*, 760–772. [CrossRef]
88. Tabatabaei, N.; Gantasala, S.; Cervantes, M. Wind Turbine Aerodynamic Modeling in Icing Condition: Three-Dimensional RANS-CFD Versus Blade Element Momentum Method. *J. Energy Resour. Technol.* **2019**, *141*, 071201. [CrossRef]
89. Caccia, F.; Guardone, A. Numerical simulations of ice accretion on wind turbine blades: Are performance losses due to ice shape or surface roughness? *Wind Energy Sci.* **2023**, *8*, 341–362. [CrossRef]
90. Yirtici, O.; Tuncer, I.H. Aerodynamic shape optimization of wind turbine blades for minimizing power production losses due to icing. *Cold Reg. Sci. Technol.* **2021**, *185*, 103250. [CrossRef]
91. Douvi, E.; Margaris, D. Aerodynamic Performance Investigation under the Influence of Heavy Rain of a NACA 0012 Airfoil for Wind Turbine Applications. *Int. Rev. Mech. Eng.* **2012**, *6*, 1228–1235. [CrossRef]
92. Douvi, E.; Margaris, D.; Lazaropoulos, S.; Svanas, S. Experimental and Computational Study of the Effects of Different Liquid Water Content on the Aerodynamic Performance of a NACA 0012 Airfoil at Low Reynolds Number. In Proceedings of the 5th International Conference on Experiments/Process/System Modeling/Simulation/Optimization (5th IC-EpsMsO), Athens, Greece, 3–6 July 2013.
93. Cao, Y.; Wu, Z.; Xu, Z. Effects of rainfall on aircraft aerodynamics. *Prog. Aerosp. Sci.* **2014**, *71*, 85–127. [CrossRef]
94. Douvi, E.; Margaris, D.; Lazaropoulos, S.; Svanas, S. Low Reynolds Number Investigation of the Flow over a NACA 0012 airfoil at Different Rainfall Rates. *Int. Rev. Mech. Eng.* **2013**, *7*, 625–632. [CrossRef]
95. Rhode, R. Some Effects on Rainfall on Flight of Airplanes and on Instrument Indications. NACA-TN-803. 1941. Available online: <https://ntrs.nasa.gov/api/citations/19930080785/downloads/19930080785.pdf> (accessed on 26 September 2023).
96. Dunham, R.; Bezos, G.; Gentry, G.; Melson, E. Two-dimensional wind tunnel tests of a transport-type airfoil in a water spray. In Proceedings of the AIAA 23rd Aerospace Sciences Meeting, Reno, NV, USA, 14–17 January 1985. [CrossRef]
97. Hastings, E.; Manuel, G. Scale-Model Tests of Airfoils in Simulated Heavy Rain. *J. Aircraft* **1985**, *22*, 536–540. [CrossRef]
98. Haines, P.; Luers, J. Aerodynamic Penalties of Heavy Rain on Landing Airplanes. *J. Aircraft* **1983**, *20*, 111–119. [CrossRef]
99. Bilanin, A. Scaling Laws for Testing of High Lift Airfoils Under Heavy Rainfall. In Proceedings of the AIAA 23rd Aerospace Science Meeting, Reno, NV, USA, 14–17 January 1985. [CrossRef]
100. Thompson, B.E.; Jang, J. Aerodynamic Efficiency of Wings in Rain. *J. Aircraft* **1996**, *33*, 1047–1053. [CrossRef]
101. Wan, T.; Wu, S.W. Aerodynamic Analysis Under the Influence of Heavy Rain. *J. Aeronaut. Astronaut. Aviat.* **2009**, *41*, 173–180.

102. Zhang, R.M.; Cao, Y.H. Study of Aerodynamics Characteristics of an Airfoil in Rain. *J. Aerosp. Power* **2010**, *25*, 2064–2069.
103. Hansman, J.; Craig, A. Low Reynolds Number Tests of NACA 64-210, NACA 0012, and Wortman FX67-K170 Airfoils in Rain. *J. Aircraft* **1987**, *24*, 559–566. [[CrossRef](#)]
104. World Development Indicators (WDI). Average Precipitation in Depth (mm per year). Food and Agriculture Organization. 2020. Available online: <https://databank.worldbank.org/reports.aspx?source=2&type=metadata&series=AG.LND.PRC.PMM> (accessed on 23 March 2023).
105. Corrigan, R.; DeMiglio, R. *Effect of Precipitation on Wind Turbine Performance*; NASA Lewis Research Center: Cleveland, OH, USA, 1985. [[CrossRef](#)]
106. Valentine, J.R.; Decker, R.A. A Lagrangian-Eulerian Scheme for Flow around an Airfoil in Rain. *Int. J. Multiph. Flow* **1995**, *21*, 639–648. [[CrossRef](#)]
107. Durst, F.; Durst, F.; Milojevic, D.; Schonung, B. Eulerian and Lagrangian predictions of particulate two-phase flows: A numerical study. *Appl. Math. Model.* **1984**, *8*, 101–115. [[CrossRef](#)]
108. Luers, J. Rain influences on a wind turbine theoretical development and applications. In Proceedings of the AIAA 23rd Aerospace Sciences Meeting, Reno, NV, USA, 14–17 January 1985. [[CrossRef](#)]
109. Cai, M.; Abbasi, E.; Arastoopour, H. Analysis of the Performance of a Wind-Turbine Airfoil under Heavy-Rain Conditions Using a Multiphase Computational Fluid Dynamics Approach. *Ind. Eng. Chem. Res.* **2013**, *52*, 3266–3275. [[CrossRef](#)]
110. Douvi, E.; Margaritis, D. Simulation of heavy rain flow over a NACA 0012 airfoil. In Proceedings of the 4th International Conference on Experiments/Process/System Modeling/Simulation/Optimization (4th IC-EpsMsO), Athens, Greece, 6–9 July 2011.
111. Cohan, A.C.; Arastoopour, H. Numerical simulation and analysis of the effect of rain and surface property on wind-turbine airfoil performance. *Int. J. Multiph. Flow* **2016**, *81*, 46–53. [[CrossRef](#)]
112. Arastoopour, H.; Cohan, A.C. CFD simulation of the effect of rain on the performance of horizontal wind turbines. *AIChE J.* **2017**, *63*, 5375–5383. [[CrossRef](#)]
113. Wu, S.; Sun, H.; Zheng, X. A numerical study on dynamic characteristics of 5 MW floating wind turbine under wind-rain conditions. *Ocean Eng.* **2022**, *262*, 112095. [[CrossRef](#)]
114. Wu, S.; Sun, H.; Li, X. Response of 5 MW Floating Wind Turbines to Combined Action of Wind and Rain. *J. Mar. Sci. Eng.* **2022**, *10*, 284. [[CrossRef](#)]
115. Anh, N.T.; Duc, N.H. A study on power output of horizontal-axis wind turbines under rain. *Vietnam J. Sci. Technol.* **2019**, *57*, 356–365. [[CrossRef](#)]
116. Anh, N.T.; Duc, N.H. Effect Analysis of Performance and Pitch Controller Operation for Wind Turbine under Rain. *GMSARN Int. J.* **2022**, *16*, 339–347.
117. Douvi, E.; Douvi, D.; Pylarinos, D.; Margaritis, D. Effect of Rain on the Aerodynamic Performance of a Horizontal Axis Wind Turbine—A Computational Study. *Int. J. Energetica* **2021**, *6*, 35–43. [[CrossRef](#)]
118. Douvi, E.; Margaritis, D. Hydrodynamic Analysis of a Horizontal Axis Tidal Turbine, Based on the Blade Element Momentum Theory. In Proceedings of the 7th International Conference on “Experiments/Process/System Modeling/Simulation/Optimization” (7th IC-EPSMSO), Athens, Greece, 5–8 July 2017.
119. Punge, H.; Kunz, M. Hail observations and hailstorm characteristics in Europe: A review. *Atmos. Res.* **2016**, *176–177*, 159–184. [[CrossRef](#)]
120. Wang, P.K. *Motions of Ice Hydrometeors in the Atmosphere: Numerical Studies and Implications*; Springer Nature: Singapore, 2020. [[CrossRef](#)]
121. Letson, F.; Barthelmie, R.; Pryor, S. Radar-derived precipitation climatology for wind turbine blade leading edge erosion. *Wind Energy Sci.* **2020**, *5*, 331–347. [[CrossRef](#)]
122. Fiore, G.; Fujiwara, G.; Selig, M. A damage assessment for wind turbine blades from heavy atmospheric particles. In Proceedings of the 53rd AIAA Aerospace Sciences Meeting, Kissimmee, FL, USA, 5–9 January 2015. [[CrossRef](#)]
123. Douvi, D.; Georgakopoulos, A.-G.; Lekkas, D.; Douvi, E.; Margaritis, D. Aerodynamic degradation of a three-bladed horizontal axis wind turbine operating during a hailstorm. In Proceedings of the 8th International Conference on “Experiments/Process/System Modeling/Simulation/Optimization” (8th IC-EPSMSO), Athens, Greece, 3–6 July 2019.
124. Douvi, D.; Douvi, E.; Plessas, D.K.; Margaritis, D.P. Numerical Simulation of NACA 0012 Airfoil Operating under Hailstorm Conditions. *Int. J. New Technol. Res.* **2021**, *7*, 73–80. [[CrossRef](#)]
125. Douvi, D.; Douvi, E. Investigation into the impact of hailstorm on the aerodynamic characteristics of S809 airfoil: A comprehensive computational analysis. In Proceedings of the 10th International Conference on “Experiments/Process/System Modeling/Simulation/Optimization” (10th IC-EPSMSO), Loutraki, Greece, 5–8 July 2023.
126. Douvi, D.; Douvi, E.; Margaritis, D. The Operation of a Three-Bladed Horizontal Axis Wind Turbine under Hailstorm Conditions—A Computational Study Focused on Aerodynamic Performance. *Inventions* **2022**, *7*, 2. [[CrossRef](#)]
127. Khalfallah, M.G.; Koliub, A.M. Effect of dust on the performance of wind turbines. *Desalination* **2007**, *209*, 209–220. [[CrossRef](#)]
128. Khakpour, Y.; Bardakji, S.; Nair, S. Aerodynamic performance of wind turbine blades in dusty environments. In Proceedings of the ASME 2007 International Mechanical Engineering Congress and Exposition, IMECE2007, Seattle, WA, USA, 11–15 November 2007. [[CrossRef](#)]
129. Al-Khayat, M.; Al-Rasheedi, M.; Gueymard, C.A.; Haupt, S.E.; Kosović, B.; Al-Qattan, A.; Lee, J.A. Performance analysis of a 10-MW wind farm in a hot and dusty desert environment. Part 2: Combined dust and high-temperature effects on the operation of wind turbines. *Sustain. Energy Technol. Assess.* **2021**, *47*, 101461. [[CrossRef](#)]

130. Ren, N.-X.; Ou, J.-P. Dust Effect on the Performance of Wind Turbine Airfoils. *J. Electromagn. Waves Appl.* **2009**, *1*, 102–107. [[CrossRef](#)]
131. Li, D.; Li, R.; Yang, C.; Wang, X. Effects of Surface Roughness on Aerodynamic Performance of a Wind Turbine Airfoil. In Proceedings of the 2010 Asia-Pacific Power and Energy Engineering Conference (APPEEC 2010), Chengdu, China, 28–31 March 2010.
132. Salem, H.; Diab, A.; Ghoneim, Z. CFD Simulation and Analysis of Performance Degradation of Wind Turbine Blades in Dusty Environments. In Proceedings of the 2013 International Conference on Renewable Energy Research and Applications (ICRERA 2013), Madrid, Spain, 20–23 October 2013. [[CrossRef](#)]
133. Wu, P.; Li, C.; Li, Z. Numerical Simulation of Influence with Surface Contamination on Aerodynamic Performance of Dedicated Wind Turbine Airfoil. *Adv. Mater. Res.* **2013**, *724–725*, 572–575. [[CrossRef](#)]
134. Fiore, G.; Selig, M. A Simulation of Operational Damage for Wind Turbine Blades. In Proceedings of the 32nd AIAA Applied Aerodynamics Conference, Atlanta, GA, USA, 16–20 June 2014. [[CrossRef](#)]
135. Fiore, G.; Selig, M. Simulation of Damage for Wind Turbine Blades Due to Airborne Particles. *Wind Eng.* **2015**, *39*, 399–418. [[CrossRef](#)]
136. Fiore, G.; Selig, M. Optimization of Wind Turbine Airfoils Subject to Particle Erosion. In Proceedings of the 33rd AIAA Applied Aerodynamics Conference, Dallas, TX, USA, 22–26 June 2015. [[CrossRef](#)]
137. Fiore, G.; Selig, M. Time marching simulations of wind turbine blades subject to particle erosion. In Proceedings of the 54th AIAA Aerospace Sciences Meeting, San Diego, CA, USA, 4–8 January 2016. [[CrossRef](#)]
138. Diab, A.; Alaa, M.; Hossam El-Din, A.; Salem, H.; Ghoneim, Z. Performance Degradation of Wind Turbine Airfoils due to Dust Contamination: A Comparative Numerical Study. In Proceedings of the ASME Turbo Expo 2015: Turbine Technical Conference and Exposition, Volume 9: Oil and Gas Applications, Supercritical CO<sub>2</sub> Power Cycles, Wind Energy, Montreal, QC, Canada, 15–19 June 2015. [[CrossRef](#)]
139. Srinivasan, S.; Surasani, V.K. CFD Analysis of Effects of Surface Fouling on Wind Turbine Airfoil Profiles. *Int. J. Power Energy Eng. Spec. Issue Energy Syst. Dev.* **2015**, *4*, 1–11.
140. Jafari, K.; Djavareshkian, M.; Feshalami, B. The Effects of Different Roughness Configurations on Aerodynamic Performance of Wind Turbine Airfoil and Blade. *Int. J. Renew. Energy Dev.* **2017**, *6*, 273–281. [[CrossRef](#)]
141. Zidane, I.; Saqr, K.; Swadener, G.; Ma, X.; Shehadeh, M. Computational Fluid Dynamics Study of Dusty Air Flow Over NACA 63415 Airfoil for Wind Turbine Applications. *J. Teknol.* **2017**, *79*, 1–6. [[CrossRef](#)]
142. Han, W.; Kim, J.; Kim, B. Effects of contamination and erosion at the leading edge of blade tip airfoils on the annual energy production of wind turbines. *Renew. Energy* **2018**, *115*, 817–823. [[CrossRef](#)]
143. Chen, S.; Agarwal, R.K. Numerical Investigation of Wind Turbine Airfoils under Clean and Dusty Air Conditions. In Proceedings of the AIAA AVIATION 2020 FORUM, St. Louis, MO, USA, 15–19 June 2020. [[CrossRef](#)]
144. Guo, T.; Jin, J.; Lu, Z.; Zhou, D.; Wang, T. Aerodynamic Sensitivity Analysis for a Wind Turbine Airfoil in an Air-Particle Two-Phase Flow. *Appl. Sci.* **2019**, *9*, 3909. [[CrossRef](#)]
145. ElMessiry, Y.; Kandil, H.; Abd-Elhady, M.S. Effect of surface contamination on the wind turbine performance. *Wind Eng.* **2021**, *45*, 505–517. [[CrossRef](#)]
146. Douvi, D.; Margaritis, D.; Davaris, A. Aerodynamic Performance of a NREL S809 Airfoil in an Air–Sand Particles Two Phase Flow. In Proceedings of the 7th International Conference “Scientific Computing to Computational Engineering” (7th IC-SCCE), Athens, Greece, 6–9 July 2016.
147. Douvi, D.; Margaritis, D.; Davaris, A.E. Aerodynamic Performance of a NREL S809 Airfoil in an Air–Sand Particle Two-Phase Flow. *Computation* **2017**, *5*, 13. [[CrossRef](#)]
148. Douvi, D.; Douvi, E.; Margaritis, D. Computational Study of NACA 0012 Airfoil in Air-Sand Particle Two-Phase Flow at Reynolds Number of  $Re = 1.76 \times 10^6$ . *Int. J. New Technol. Res.* **2019**, *5*, 101–108. [[CrossRef](#)]
149. Douvi, D.; Margaritis, D. Numerical simulation of NACA 0012 airfoil in air phase flow and in high concentration air–sand particles two-phase flow. In Proceedings of the 8th International Conference from “Scientific Computing to Computational Engineering” (8th IC-SCCE), Athens, Greece, 4–7 July 2018.
150. Douvi, D.; Douvi, E.; Margaritis, D. Aerodynamic Performance of a Horizontal Axis Wind Turbine Operating with Dust—A Computational Study. *Inventions* **2023**, *8*, 3. [[CrossRef](#)]
151. Marten, D.; Wendler, J.; Pechlivanoglou, G.; Nayeri, C.; Paschereit, C. QBlade: An Open Source Tool for Design and Simulation of Horizontal and Vertical Axis Wind Turbines. *Int. J. Emerg. Technol. Adv. Eng.* **2013**, *3*, 264–269.
152. Zare, J.; Hosseini, S.; Rastan, M. NREL Phase VI wind turbine in the dusty environment. *arXiv* **2023**, arXiv:2304.06285.
153. Corten, G.; Veldkamp, H. *Insects Cause Double Stall*; EWEC: Copenhagen, Denmark, 2001.
154. BladeCleaning. 2017. Available online: <http://www.bladecleaning.com/> (accessed on 4 August 2023).
155. Petrone, G.; de Nicola, C.; Quagliarella, D.; Witteveen, J.; Iaccarino, G. Wind Turbine Performance Analysis Under Uncertainty. In Proceedings of the 49th AIAA Aerospace Sciences Meeting Including the New Horizons Forum and Aerospace Exposition, Orlando, FL, USA, 4–7 January 2011. [[CrossRef](#)]
156. Lachmann, G. *Aspects of Insect Contamination in Relation to Laminar Flow Aircraft*; Aeronautical Research Center: London, UK, 1960.
157. Janiszewska, J.; Rastan, R.R.; Hoffmann, M.; Gregorek, G. *Effects of Grit Roughness and Pitch Oscillations on the LS(1)-0417MOD Airfoil*; National Renewable Energy Laboratory: Golden, CO, USA, 1996. [[CrossRef](#)]
158. Janiszewska, J.; Reuss Ramsay, R.R.; Hoffmann, M.; Gregorek, G. *Effects of Grit Roughness and Pitch Oscillations on the S814 Airfoil*; National Renewable Energy Laboratory: Golden, CO, USA, 1996. [[CrossRef](#)]

159. Hoffman, M.; Reuss, R.; Gregorek, G. *Effects of Surface Roughness and Vortex Generators on the NACA 4415 Airfoil*, NREL/TP-442-7815; National Renewable Energy Laboratory: Golden, CO, USA, 1996. [[CrossRef](#)]
160. Ramsay, R.; Hoffman, M.; Gregorek, G. *Effects of Grit Roughness and Pitch Oscillations on the S801 Airfoil*, NREL/TP-442-7818; National Renewable Energy Laboratory: Golden, CO, USA, 1996. [[CrossRef](#)]
161. Reuss, R.; Hoffman, M.; Gregorek, G. *Effects of Surface Roughness and Vortex Generators on the S809 Airfoil*, NREL/TP-442-7817; National Renewable Energy Laboratory: Golden, CO, USA, 1995. [[CrossRef](#)]
162. Hoffmann, M.; Reuss Ramsay, R.; Gregorek, G. *Effects of Surface Roughness and Vortex Generators on the S813 Airfoil*, NREL/TP-442-7815; National Renewable Energy Laboratory: Golden, CO, USA, 1996.
163. Ferrer, E.; Munduate, X. CFD Predictions of Transition and Distributed Roughness Over a Wind Turbine Airfoil. In Proceedings of the 47th AIAA Aerospace Sciences Meeting Including the New Horizons Forum and Aerospace Exposition, Orlando, FL, USA, 5–8 January 2009. [[CrossRef](#)]
164. Wilcox, B.; White, E.; Maniaci, D. *Roughness Sensitivity Comparisons of Wind Turbine Blade Sections*; Sandia National Laboratories: Albuquerque, NM, USA, 2017. [[CrossRef](#)]
165. Ehrmann, R.; Wilcox, B.; White, E.; Maniaci, D. *Effect of Surface Roughness on Wind Turbine Performance*; Sandia National Laboratories: Albuquerque, NM, USA, 2017. [[CrossRef](#)]
166. Yu, X.; Yan, L. High Humidity Aerodynamic Effects Study on Offshore Wind Turbine Airfoil/Blade Performance Through CFD Analysis. In Proceedings of the ASME Turbo Expo 2017: Turbomachinery Technical Conference and Exposition Volume 9: Oil and Gas Applications, Supercritical CO2 Power Cycles, Wind Energy, Charlotte, NC, USA, 26–30 June 2017.
167. Yue, W.; Xue, Y.; Liu, Y. High Humidity Aerodynamic Effects Study on Offshore Wind Turbine Airfoil/Blade Performance through CFD Analysis. *Int. J. Rotating Mach.* **2017**, *2017*, 7570519. [[CrossRef](#)]
168. Sathiesh Kumar, V.; Vasa, N.; Sarathi, R. Detecting salt deposition on a wind turbine blade using laser-induced breakdown spectroscopy technique. *Appl. Phys. A* **2013**, *112*, 149–153. [[CrossRef](#)]
169. Yokoyama, S. Lightning protection of wind turbine blades. *Electr. Power Syst. Res.* **2013**, *94*, 3–9. [[CrossRef](#)]
170. Huang, S.-L.; Chen, J.-F.; Liang, T.-J.; Su, M.-S.; Chen, C.-Y. Prediction of salt contamination in the rotating blade of wind turbine under lightning strike occurrence using fuzzy c-means and k-means clustering approaches. *IET Sci. Meas. Technol.* **2020**, *14*, 91–97. [[CrossRef](#)]
171. Wright, J.M.; Colling, A. *Seawater: Its Composition, Properties and Behaviour*, 2nd ed.; Bearman, G., Ed.; Butterworth-Heinemann: Oxford, UK, 1995.

**Disclaimer/Publisher’s Note:** The statements, opinions and data contained in all publications are solely those of the individual author(s) and contributor(s) and not of MDPI and/or the editor(s). MDPI and/or the editor(s) disclaim responsibility for any injury to people or property resulting from any ideas, methods, instructions or products referred to in the content.